



Strathprints Institutional Repository

Galindo-Rosales, Francisco J and Alves, M.A. and Oliveira, Monica (2013) *Microdevices for extensional rheometry of low viscosity elastic liquids : a review*. *Microfluidics and Nanofluidics*, 14 (1-2). pp. 1-19. ISSN 1613-4982

Strathprints is designed to allow users to access the research output of the University of Strathclyde. Copyright © and Moral Rights for the papers on this site are retained by the individual authors and/or other copyright owners. You may not engage in further distribution of the material for any profitmaking activities or any commercial gain. You may freely distribute both the url (<http://strathprints.strath.ac.uk/>) and the content of this paper for research or study, educational, or not-for-profit purposes without prior permission or charge.

Any correspondence concerning this service should be sent to Strathprints administrator: <mailto:strathprints@strath.ac.uk>

2 **Microdevices for extensional rheometry of low viscosity**
3 **elastic liquids: a review**

4 **F. J. Galindo-Rosales · M. A. Alves ·**
5 **M. S. N. Oliveira**

6 Received: 15 March 2012 / Accepted: 27 June 2012
7 © Springer-Verlag 2012

8 **Abstract** Extensional flows and the underlying stability/
9 instability mechanisms are of extreme relevance to the
10 efficient operation of inkjet printing, coating processes and
11 drug delivery systems, as well as for the generation of
12 micro droplets. The development of an extensional rhe-
13 ometer to characterize the extensional properties of low
14 viscosity fluids has therefore stimulated great interest of
15 researchers, particularly in the last decade. Microfluidics
16 has proven to be an extraordinary working platform and
17 different configurations of potential extensional microrhe-
18 ometers have been proposed. In this review, we present an
19 overview of several successful designs, together with a
20 critical assessment of their capabilities and limitations.

21
22 **Keywords** Extensional flow · Filament stretching ·
23 Filament thinning · Diluted polymer solution · Rheometry ·
24 Microfluidics · Extensional viscosity · Viscoelasticity

25 **1 Introduction**

26 Extensional deformation plays a significant role in many
27 processing operations of polymer melts and solutions.
28 Examples include extrusion, coating flows, contraction
29 flows, fiber spinning, blow molding, film blowing, and foam

production (Gaudet and McKinley 1998; Zheng et al. 30
2011). Since extensional flows strongly orient polymer 31
molecules and asymmetric particles, the presence of regions 32
of strong extensional flow in processing operations can have 33
a major effect on final product properties (Macosko 1994). 34
Moreover, in the food industry, the extensional properties 35
are also important in various stages of the product life cycle, 36
from the initial stage of formulation and process design, to 37
process and quality control of products, to the final stage 38
of sensory perception of the product by the consumer 39
(Padmanabhan and Bhattacharya 1993; Padmanabhan 40
1995; Funami 2011). There are also other industrial and 41
commercial applications, such as agrochemical spraying, 42
inkjet printing, turbulent drag reduction or enhanced oil 43
recovery, in which the extensional properties of the working 44
fluids are of extreme importance (Oliveira et al. 2006; 45
Rothstein 2008), since viscoelastic fluids frequently exhibit 46
strong extensional thickening well beyond the Trouton ratio 47
(Trouton 1906) found for Newtonian fluids ($Tr = \eta_e/\eta = 3$ 48
for axisymmetric elongation, or $Tr = \eta_e/\eta = 4$ for planar 49
elongation). Therefore, in order to accurately model these 50
materials, detect subtle dissimilarities in their composition, 51
and to describe or predict the processing conditions that will 52
optimize fluid flow or characteristics of the final product, a 53
thorough rheological characterization of materials in both 54
shear and extensional flow conditions is recommended 55
(Barnes et al. 1993). 56

Despite the recognized importance of extensional flows, 57
we still face an unbalanced scenario in the field of rhe- 58
ometry, with the rheological characterization under simple 59
shear flow being by far the most abundant in rheology, to 60
such an extent that it often becomes a synonym for rhe- 61
ology in general (Dukhin and Zelenev 2010). However, it 62
is not possible to describe adequately the highly complex 63
dependency on both strain and strain rate experienced by a 64

A1 F. J. Galindo-Rosales (✉) · M. A. Alves
A2 Departamento de Engenharia Química, Centro de Estudos
A3 de Fenómenos de Transporte (CEFT), Faculdade de Engenharia
A4 da Universidade do Porto, Rua Dr. Roberto Frias s/n,
A5 4200-465 Porto, Portugal
A6 e-mail: galindo@fe.up.pt; curro@galindorosales.com

A7 M. S. N. Oliveira
A8 Department of Mechanical and Aerospace Engineering,
A9 University of Strathclyde, Glasgow G1 1XJ, UK

65 fluid element of a viscoelastic material in a strong exten-
 66 sional flow using exclusively a shear rheological charac-
 67 terization. This has been the motivation which has been
 68 fueling extensive research in the past decades to understand
 69 the extensional flow behavior of different materials.
 70 Research in this topic has involved a synergistic effort in
 71 theoretical analysis of extensional flow behavior in order to
 72 determine the critical parameters and identify the optimal
 73 flow kinematics, and in improving the experimental design
 74 of extensional rheometers in order to successfully impose
 75 the desired kinematics (Nijenhuis et al. 2007). Ideally, a
 76 pure extensional (or shear-free) flow, in which the rate-of-
 77 strain tensor ($\mathbf{D} = \frac{1}{2}[\nabla\mathbf{v} + \nabla\mathbf{v}^T]$) has only non-zero values
 78 on the diagonal elements ($\frac{\partial u_i}{\partial x_j} = 0, \forall i \neq j$) and consequently
 79 the vorticity tensor is null ($\mathbf{w} = \frac{1}{2}[\nabla\mathbf{v} - \nabla\mathbf{v}^T] = \mathbf{0}$), would
 80 allow us to characterize properly the extensional properties
 81 of the fluid. However, due to difficulties associated with
 82 imposing purely extensional deformations, the develop-
 83 ment of instrumentation able to carry out extensional vis-
 84 cosity measurements is still a challenging task. Twenty five
 85 years ago, Bird et al. (1987) summarized this idea in the
 86 following statement: “Unlike the situation for shear flows
 87 where there are numerous methods available for measuring
 88 material functions of a wide variety of polymeric liquids,
 89 techniques for measuring the kinds of shear-free flow
 90 material functions have been developed only for polymer
 91 melts and high-viscosity solutions”. In spite of the diffi-
 92 culties in generating homogeneous extensional flows,
 93 avoiding shear components and controlling the strain histo-
 94 ry of the material elements (Petrie 1997; Anna et al.

2001; Ríos et al. 2002; Bänsch et al. 2004), especially with
 low viscosity liquids, significant improvements have been
 achieved over the last 25 years. As a consequence of this
 active research, a family of extensional rheometers and
 detachable extensional rheometer fixtures for use in com-
 mercial torsional rheometers are nowadays available on the
 market and allow the user to cover a wide range of mate-
 rials from low to highly viscous fluids, and from polymer
 solutions to polymer melts, as schematically illustrated in
 Fig. 1. Most of the apparatus developed for measuring the
 extensional viscosity are more appropriate for high-vis-
 cosity materials, such as polymer melts (Münstedt 1979;
 Meissner 1985a, b; Maia et al. 1999; Schweizer 2000;
 Sentmanat et al. 2005; Göttfert 2011; Franck 2011), mainly
 due to the fact that the high viscosity of such polymer melts
 allows the preparation of homogeneous sheets or rods of
 material that are subsequently subjected to an elongation
 process under conditions of either constant deformation
 rate or constant stress (McKinley and Sridhar 2002). On the
 other hand, methods for determining the extensional
 properties of less viscous complex fluids, such as dilute
 polymer solutions, are more limited and in most cases are
 still under active development.

The opposed jet rheometer developed by Fuller et al.
 (1987), commercialized as the RFX instrument by Rheo-
 metrics (now TA Instruments), was able to characterize the
 extensional properties of low viscosity fluids. This tech-
 nique was used extensively to measure the extensional
 properties of various aqueous solutions in the 1990s (e.g.
 Hermansky and Boger 1995; Ng et al. 1996). However,
 since large deformation rates were required to induce

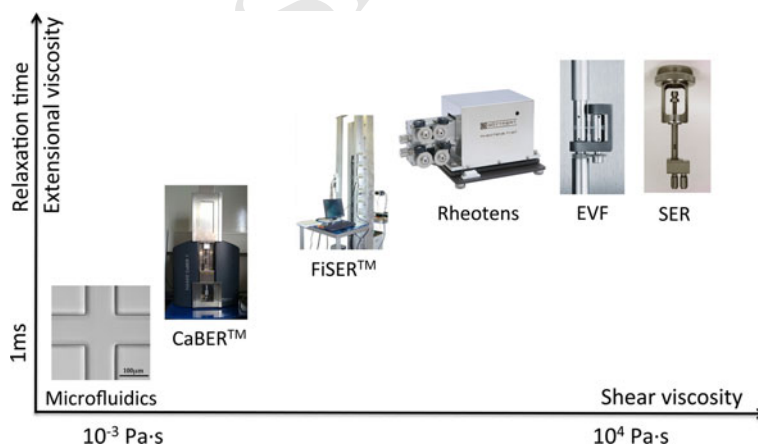


Fig. 1 Range of available extensional rheometers: operability diagram in terms of the fluid shear viscosity and extensional viscosity (or shear viscosity and relaxation time) of the materials that are typically measured. The CaBER™ device was developed by the Cambridge Polymer Group (MA, USA) and is commercialized by ThermoFischer (MA, USA). The FiSER™ device illustrated was developed and commercialized by the Cambridge Polymer Group. The Rheotens 71.97 device illustrated is commercialized by Göttfert (Germany).

The extensional viscosity fixture (EVF) is commercialized by TA Instruments (DE, USA). The Sentmanat Extensional Rheometer (SER) fixture was developed by Dr. M. Sentmanat and is commercialized by Xpansion Instruments (OH, USA) and likewise the EVF can be used as a detachable fixture on a commercial rotational rheometer. The images of FiSER™, Rheotens, EVF and SER are reproduced with permission of Cambridge Polymer Group, Göttfert, TA Instruments and Xpansion Instruments, respectively

126 significant viscoelastic effects, the inertial stresses in the
 127 fluid at such rates can completely mask the viscoelastic
 128 stresses resulting from molecular deformation, leading to
 129 erroneous results (Dontula et al. 1997; Rodd et al. 2005b).
 130 Nevertheless, although the RFX instrument is nowadays
 131 out of the market as a standalone device, it is still a subject
 132 of research and recently a new opposed-nozzle fixture, that
 133 can be mounted onto a controlled strain rheometer, was
 134 developed by Soulages et al. (2009a).

135 Among the plethora of techniques developed for
 136 extensional characterization of mobile liquids, reviewed by
 137 Gupta and Sridhar (1988) and McKinley and Sridhar
 138 (2002), filament stretching rheometry has sparked off great
 139 interest since the pioneering work of Matta and Tytus
 140 (1990) and Bazilevsky et al. (1990). In just one decade it
 141 matured to such an extent that in 2001 it was already
 142 considered as an accurate method for characterizing the
 143 response of viscoelastic fluids and, in particular, of viscous
 144 dilute polymer solutions, almost achieving an ideal uni-
 145 axial extensional deformation (Anna et al. 2001). Accord-
 146 ing to Sridhar (2000) it represented the culmination of
 147 about four decades of intense research in the development
 148 of a suitable extensional rheometer. A major advantage is
 149 that the velocity field far from the rigid endplates is
 150 essentially one-dimensional and purely extensional
 151 (Schultz and Davis 1982). Over the past two decades dif-
 152 ferent filament stretching configurations have been pro-
 153 posed for generating such flows, but two among those have
 154 showed enhanced performance for rheometric purposes
 155 (McKinley et al. 2001):

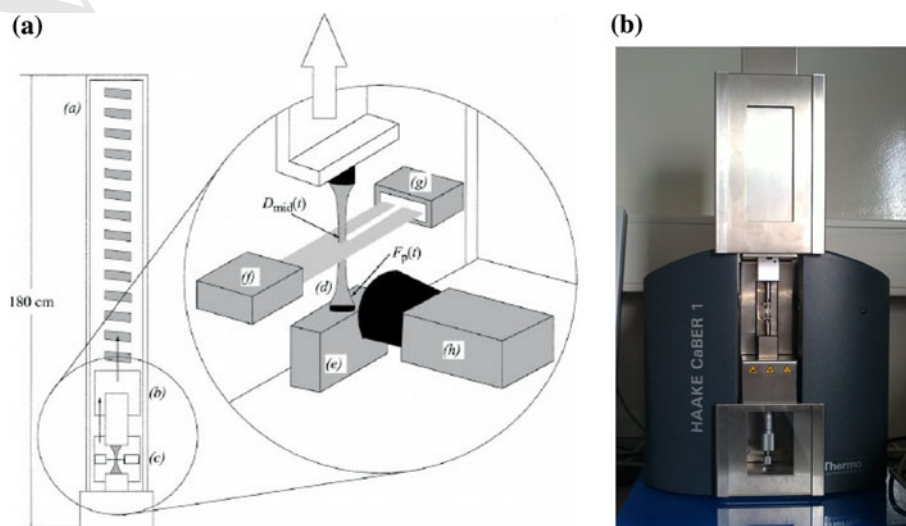
156 • The filament stretching extensional rheometer (FiS-
 157 ERTM) illustrated in Fig. 2a imposes an exponential
 158 velocity to the upper plate in order to induce a uniaxial
 159 extensional flow with constant strain rate, rather than
 160 constant tensile force, as in the original concept of

161 Matta and Tytus (1990). The temporal evolution of the
 162 tensile force exerted by the fluid column on the bottom
 163 endplate and of the filament radius at the axial mid-
 164 plane of the filament are both measured and used to
 165 compute the transient extensional viscosity (McKinley
 166 et al. 2001). A more reliable version of the FiSERTM
 167 can use a real-time algorithm to control the upper plate
 168 velocity in order to achieve the desired exponential
 169 decay of the filament diameter at the midpoint (Anna
 170 et al. 1999).

171 • The capillary breakup extensional rheometer
 172 (CaBERTM), based on the ideas of Bazilevsky et al.
 173 (1990), imposes an extensional step strain of order
 174 unity and the filament subsequently thins under the
 175 influence of capillary forces without additional kine-
 176 matic input at the boundaries. Subsequently, the fluid
 177 filament undergoes a thinning process with an exten-
 178 sional strain rate defined by the extensional properties
 179 of the fluid. Large extensional strains can still be
 180 attained as the mid-region of the filament progressively
 181 necks down and eventually breaks. Typically, the only
 182 measured quantity is the time evolution of the midpoint
 183 diameter of the necking filament (see Fig. 2b) and the
 184 relaxation time is determined from the exponential
 185 decay of the filament diameter with time (McKinley
 186 et al. 2001).

187 The relative merits of the CaBERTM and FiSERTM
 188 apparatuses, as well as the dynamics of capillary thinning
 189 of Newtonian and non-Newtonian fluids have been dis-
 190 cussed thoroughly by McKinley and Tripathi (2000),
 191 McKinley and Sridhar (2002) and McKinley (2005). Even
 192 though the CaBERTM can be used to measure relaxation
 193 times of viscoelastic liquids with significantly lower vis-
 194 cosities than the FiSERTM there is still a limit of operation,
 195

Fig. 2 **a** Schematic diagram of a FiSERTM for moderately viscous materials [reprinted from Anna et al. (1999), Copyright (1999), with permission from Elsevier Science]. **b** Commercial CaBERTM 1 apparatus



196 as depicted in the CaBERTM operability diagram presented
 197 by Rodd et al. (2005b). This diagram defines a minimum
 198 limit for the measurable relaxation time around 1 ms for
 199 liquids with a shear viscosity of about 3 mPa s achievable
 200 by selecting appropriately the operating conditions, which
 201 in practical terms is very difficult to achieve due to strong
 202 inertial effects and the fact that the position of the nar-
 203 rowest part of the filament is not always matching the
 204 position of the laser micrometer. For these reasons, the use
 205 of high speed cameras for recording the filament necking
 206 process is becoming a common practice as a complemen-
 207 tary technique for evaluating the extensional properties of
 208 low viscosity fluids and for extending the limits of reliable
 209 operation for the CaBERTM (Oliveira et al. 2005, 2006;
 210 Niedzwiedz et al. 2009, 2010; Roche et al. 2011).
 211 Recently, Campo-Deaño and Clasen (2010) presented a
 212 reliable technique to measure relaxation times in extension
 213 as low as 240 μ s with the CaBERTM using a high-speed
 214 camera and a slow retraction method in order to minimize
 215 inertial oscillations originated from the acceleration of the
 216 liquid. There are also some works where micro-length
 217 scales have also been considered with the CaBERTM
 218 technique (Kojic et al. 2006; Sattler et al. 2008; Erni et al.
 219 2011) and the range of operation was analyzed theoretic-
 220 ally (Ardekani et al. 2010).

221 In spite of the ability of the filament thinning experi-
 222 ments to stretch significantly the samples, stress measure-
 223 ments indicated that the chains were not reaching their full
 224 extension (Babcock et al. 2003). Furthermore, one of the
 225 major concerns about filament stretching rheometry is
 226 related with the undesirable influence of gravitational
 227 effects, since even small gravitational forces can lead to a
 228 significant distortion of the liquid bridges (Bänsch et al.
 229 2004).

230 In recent FiSERTM experiments, the effect of pre-
 231 deformation history on the uniaxial extensional flow was
 232 analyzed (Anna and McKinley 2008). Recent experiments
 233 were carried out in the International Space Station inside
 234 the Microgravity Science Glovebox under the auspices of
 235 the NASA (SHERE in 2008 and SHERE II in 2011) in
 236 order to obtain material property measurements of the
 237 fluids using different rotational preshear histories and
 238 imposing different axial extensional rates (McKinley and
 239 Hall 2011a, b) without the undesirable effects of gravity.

240 The inherent difficulties of extensional rheometry of
 241 low-viscosity fluids due to gravitational and inertial effects
 242 can be minimized through miniaturization of rheometric
 243 instrumentation. However, the ability of macroscale sys-
 244 tems to probe the bulk rheology of a fluid at the microscale
 245 remains limited, since the scale down of some mechanical
 246 subsystems, such as torsional motors and torque transduc-
 247 ers, is impractical (Pipe and McKinley 2009). As an
 248 alternative approach, the use of microfluidics for

249 rheometric purposes is very promising and has attracted the
 250 attention of several research groups.

251 In the present article, we discuss the important recent
 252 developments on microfluidic rheometry to generate strong
 253 extensional flows and to measure bulk rheological prop-
 254 erties in extensional flow, and present a critical assessment
 255 of their capabilities and limitations of operation. This
 256 review complements the work by Pipe and McKinley
 257 (2009), which reviews bulk rheology measurements at the
 258 microscale, for shear and extensional flows, but focuses on
 259 capillary, stagnation and contraction flows.

2 Microfluidics as a platform for extensional rheometry 260

261 Microfluidics is the science and technology of systems that
 262 process or manipulate very small amounts of fluids in
 263 geometries with characteristic lengthscales ranging from
 264 tens to hundreds of micrometres, and is now established as
 265 a new field of research (Whitesides 2006). While most
 266 research in microfluidics concerns Newtonian fluids, many
 267 fluids of interest for lab-on-a-chip applications are likely to
 268 exhibit complex microstructure and non-Newtonian
 269 behavior, such as viscoelasticity (Squires and Quake 2005).
 270 The small characteristic lengthscales of microfluidics
 271 enable the generation of flows with high deformation rates
 272 while keeping the Reynolds number (Re) small. These
 273 unique flow features result in the ability to promote strong
 274 viscoelastic effects, quantified by the elasticity number (El)
 275 that scales inversely with the square of the characteristic
 276 length (L), which are highly enhanced as the scale is
 277 reduced. This effect is especially noteworthy for low vis-
 278 cosity complex fluids (e.g. inks, coating fluids, DNA
 279 solutions, etc.) (Oliveira et al. 2008b), for which the elas-
 280 ticity number may be small in macroscopic flows ($El \ll 1$),
 281 but very large at the microscale and most likely not con-
 282 cealed by flow inertia (Rodd et al. 2005a). Therefore,
 283 detailed understanding of the impact of fluid rheological
 284 properties on flows at such small scales is clearly desirable.
 285 These distinctive flow characteristics together with the
 286 development and growth of microfluidic techniques pro-
 287 vide a rich platform for rheologists to perform rheometric
 288 investigations of non-Newtonian fluid flow phenomena at
 289 small scales and new opportunities for material property
 290 characterization (Soulages et al. 2009b). Moreover, due to
 291 difficulties in the measurement of rheological properties in
 292 extensional flows at the macroscopic scale, especially for
 293 low viscosity liquids (Petrie 2006; Campo-Deaño and
 294 Clasen 2010), the use of microfluidic devices to measure
 295 bulk properties in extensional flow is a promising approach
 296 and has been an active topic of research in recent years
 297 (Pipe and McKinley 2009), examples include microfluidic
 298 implementations of the four-roll mill (Lee et al. 2007), the

299 cross-slot flow geometry (Arratia et al. 2008; Alves 2008;
300 Haward et al. 2012a), or the use of contraction flows (Rodd
301 et al. 2007; Oliveira et al. 2007a; Campo-Deaño et al.
302 2011).

303 Based on this scenario, Pipe and McKinley (2009)
304 reviewed recently that microfluidics can be used to deter-
305 mine bulk rheological properties of complex fluids, as
306 modern microrheology does using colloidal probes sus-
307 pended in the fluids (Squires and Mason 2010). Moreover,
308 a microfluidic-based rheometer-on-a-chip has a number of
309 practical advantages such as having no air–liquid interface,
310 that might be of interest for use with biological fluids and
311 fluids prone to evaporation, and additionally it could serve
312 as an online rheological sensor in many industrial pro-
313 cesses (Bandalusena et al. 2009), which is an important
314 advantage relative to microrheology. Guillot et al. (2006,
315 2008) achieved relative success in measuring shear rheo-
316 logical properties in microfluidic channels. Pipe et al.
317 (2008) were also able to measure steady shear flow curves
318 by means of a rheometer-on-a-chip containing three flush
319 mounted microelectromechanical systems (MEMS) pres-
320 sure sensors (see Fig. 3), as used in the m-VROC™
321 microfluidic shear rheometer commercialized by Rheo-
322 sense Inc. (San Ramon, CA, USA).

323 Summing up, the advent of microfluidic technology has
324 not only increased the need for rheological information
325 about diluted polymer solutions but also provided a new
326 platform for developing and testing new rheometric devi-
327 ces. In particular, microfluidic stagnation and contraction
328 flows, used for investigating the longstanding problem of
329 the extensional behavior of low viscosity viscoelastic liq-
330 uids, show great potential and are viable alternatives to
331 conventional rheological characterization techniques.
332 Additionally, it is a golden opportunity for computational
333 rheologists to incorporate and test new constitutive

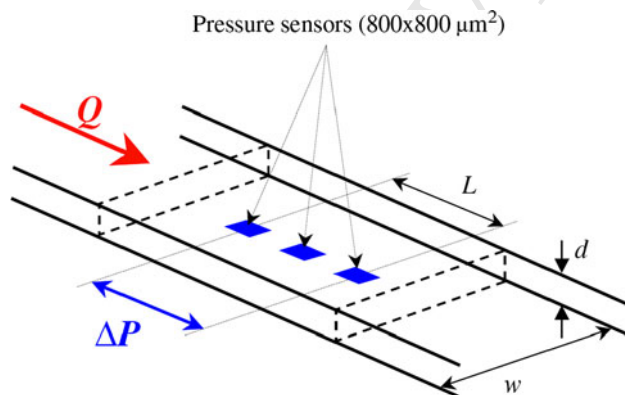


Fig. 3 Illustration of the RheoSense VROC slit microfluidic rheometer, made from Pyrex mounted on a gold-coated silicon substrate with three flush mounted MEMS pressure sensors. With kind permission from Springer Science+Business Media, Pipe et al. (2008, figure 2)

equations for viscoelastic fluid modeling in complex flows, 334
and investigate high-Weissenberg number flow conditions. 335

2.1 Microfluidic stagnation-point flows 336

A stagnation-point in a fluid flow is the location where the 337
velocity is zero, but local extension rate can be finite (free 338
stagnation point) or zero (pinned stagnation point) (Sou- 339
lages et al. 2009b). A classical application of the stagna- 340
tion-point in fluid flows is the *Pitot tube* used on a routine 341
basis for measuring the flow velocity. Recently, flows with 342
internal (or free) stagnation point, such as those generated 343
in a four-roll mill (Taylor 1934; Lagnado and Leal 1990;
Hudson et al. 2004; Pathak and Hudson 2006; Lee et al. 345
2007), cross-slot (Perkins et al. 1997; Rimmelgas et al. 346
1999; Arratia et al. 2006; Odell and Carrington 2006;
Poole et al. 2007; Alves 2008; Dylla-Spears et al. 2010) or 348
T-junctions (Link et al. 2004; Soulages et al. 2009b), are 349
increasingly popular due to the interest in understanding 350
the flow of complex fluids under strong extensional 351
deformations, and evaluating the extensional properties of 352
dilute polymer solutions in particular (Becherer et al. 353
2008). The vorticity-free state of the flow near a free 354
stagnation-point can result in large extensional deformation 355
and orientation of the microstructure of complex fluids 356
(Pipe and McKinley 2009). Another reason for the interest 357
in stagnation-point flows is their capability to trap macro- 358
molecules or microscopic objects by purely hydrodynamic 359
means while subjecting them to a strong extensional 360
deformation (Tanyeri et al. 2010, 2011), as has been done 361
with long DNA molecules (Shaqfeh 2005; Balducci et al. 362
2008; Dylla-Spears et al. 2010). 363

Theoretical modeling of stagnation-point flows has 364
proven to be particularly challenging, and despite extensive 365
experimental and theoretical investigation, some aspects of 366
these complex flows remain to be elucidated (Becherer 367
et al. 2008). In the next sections, we focus on the three 368
configurations mostly used in microfluidics for generating 369
stagnation-point flows and we summarize their capabilities 370
and limitations for characterizing extensional properties of 371
low viscosity fluids. 372

2.1.1 Microfluidic four-roll mill 373

The *four-roller apparatus* (cf. Fig. 4), commonly known as 374
four-roll mill, was invented by Taylor (1934) during his 375
investigations on the stirring process to generate emulsions 376
of two immiscible fluids. This device consists of four 377
cylinders arranged in a square configuration which rotate 378
inside a container filled with fluid. A four-roll mill has the 379
ability to generate different flow kinematics ranging from 380
pure extension, to shear, or to pure rotation, through an 381
appropriate choice of speed and direction of rotation of the 382

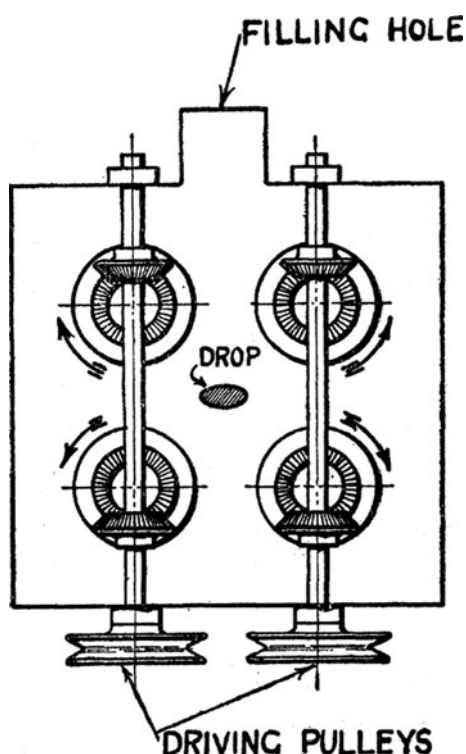


Fig. 4 Original sketch of the "four-roller apparatus". Reproduced with permission from Taylor (1934)

383 four cylindrical rollers (the apparatus of Fig. 4 is less
384 versatile because the four cylinders cannot be driven
385 independently). Among the wide variety of homogeneous
386 two-dimensional flows that can be produced with a four-
387 roll mill apparatus, the quasi-two-dimensional extensional
388 flow in the central region between the rollers is only one
389 particular case, as highlighted by Lagnado and Leal (1990).
390 Therefore, in principle, combining the capabilities of the
391 four-roll mill and the low inertia flow conditions of mi-
392 crofluidics would offer the possibility of measuring the
393 extensional properties of low viscosity fluids and analyze
394 the response of single molecules under strong extensional
395 flow. However, developing a microfluidic four-roll mill is a
396 challenging task.

397 Hudson et al. (2004) and Phelan Jr. et al. (2005)
398 developed an ingenious microfluidic design of an analog of
399 the four-roll mill, consisting of six intersecting channels
400 with asymmetric configuration (see Fig. 5). By choosing
401 the appropriate flow rate in each channel, they showed that
402 it is possible to create in this geometry a central stagnation
403 point around which the flow type could be varied from pure
404 extension to nearly pure rotation, including simple shear
405 flow conditions (Hudson et al. 2004; Pathak and Hudson
406 2006). However, this microfluidic device has two major
407 drawbacks: pure rotation cannot be obtained due to the
408 asymmetry of the geometry (Lee et al. 2007), and the
409 aspect ratio of the device (depth/width, h/w) must be

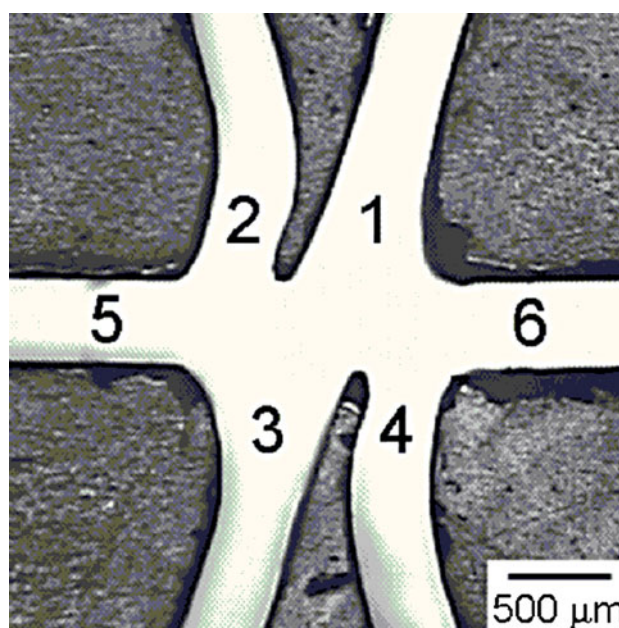


Fig. 5 Microfluidic analog of the four-roll mill proposed by Hudson et al. (2004). Reprinted with permission from Hudson et al. (2004), Copyright (2004), American Institute of Physics

greater than unity to generate substantial rotation (Hudson et al. 2004).

Lee et al. (2007) proposed another microfluidic analogue of a four-roll mill able to keep geometrical symmetry around the stagnation point and to access the full spectrum of flow types, ranging from pure rotation to pure extension, using different aspect ratios of the channel. This microfluidic four-roll mill analogue consists of four inlet and four outlet streams arranged in pairs and disposed symmetrically with regards to the central cavity, as shown in Fig. 6. In comparison with the original design of Hudson et al. (2004), the drawbacks previously mentioned were overcome, since this design is able to achieve pure rotation even with a modest aspect ratio ($h/w \approx 2$), and much lower aspect ratios can be used. Additionally, controlling the flow type becomes easier in this device.

2.1.2 Cross-slot microdevices

Among the microdevices that generate stagnation-point flows, the *cross-slot* device is probably the configuration which has attracted most attention due to its simple geometry and easy control. The standard cross-slot consists of four channels connecting at the same point, arranged orthogonally in the same plane, as illustrated in Fig. 7. The channels can have square, rectangular or circular cross-sections and the space in the chamber can vary in different configurations. When the fluid is injected in two opposing channels at the same flow rate, the opposing fluid streams

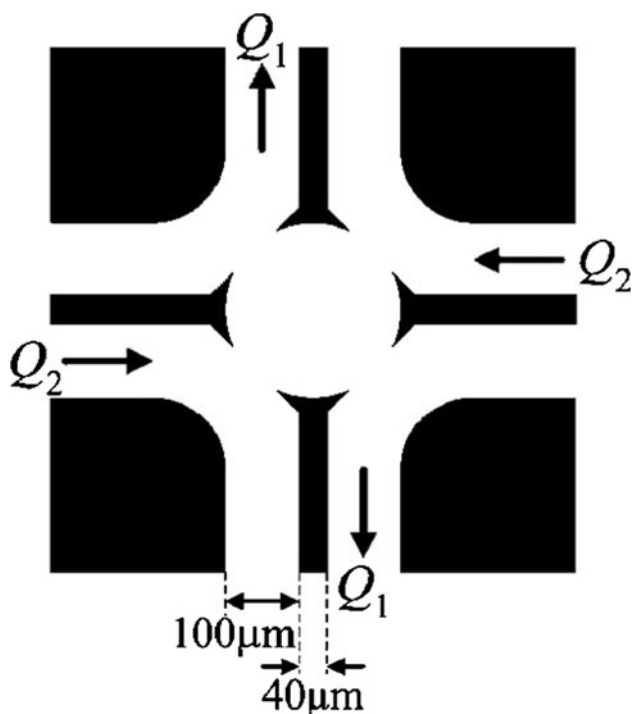


Fig. 6 Schematic diagram of a microfluidic four-roll mill device. Varying the flow rate ratio Q_2/Q_1 allows to generate all flow types. Reprinted with permission from Lee et al. (2007), Copyright (2007), American Institute of Physics

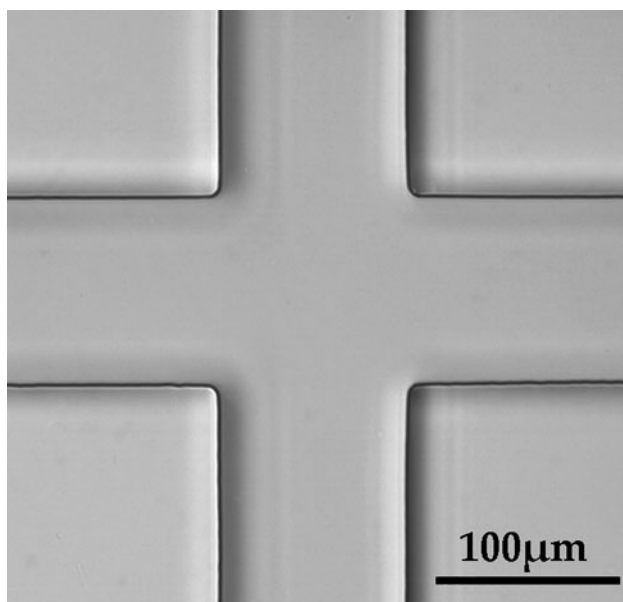


Fig. 7 Bright field image of a standard cross-slot microchannel

collide to produce a well-defined stagnation point located at the center of the geometry (if the exit flow rates are also the same), and a strong planar extensional flow is produced in the orthogonal direction while the fluid exits the chamber. Due to these flow characteristics, the standard cross-slot has been used to trap and stretch single molecules, as

done by Dylla-Spears et al. (2010) who investigated the behavior of double-stranded genomic DNA for detection of target sequences along the DNA backbone. The cross-slot microdevice has also been used for analyzing elastic instabilities of polymeric solutions in a planar extensional flow (Arratia et al. 2006; Haward et al. 2012a), which can also be used to induce *enhanced mixing* at microscale (Squires and Quake 2005).

Based on the standard cross-slot configuration, Odell and Carrington (2006) proposed the combination of oscillatory flow with a stagnation point extensional flow field to measure the extensional viscosity of low viscosity fluids. Their extensional flow oscillatory rheometer (EFOR), shown in Fig. 8, consists of a standard cross-slot cell, where the planar extension is created, having four micro-pumps positioned at the end of each channel. These micro-pumps are driven electronically and can induce any cyclic or constant flow rate profile as required, thus controlling the imposed strain and strain-rate. It is also equipped with pressure transducers in two of its limbs to record flow resistance measurements and thus provide information on the apparent extensional viscosity. In addition, by means of an optical probe to measure birefringence, the flow field stability, microstructure and molecular orientation data can be recorded simultaneously. This opto-microfluidic technique has been used in the characterization of both the shear and the extensional response of low-viscosity polymer solutions (Haward 2010; Haward et al. 2011). Moreover, the oscillatory extensional flow technique has potential applications beyond the measurement of extensional viscosity of low viscosity fluids (Odell and Carrington 2006). For instance, it can be used to investigate thermo-mechanical degradation of polymers, or even model extensional and shear flows occurring in porous media flows in tertiary oil-recovery by means of imposing customized flow profiles. Up to the current date the EFOR seems to be the paradigm of the combination between microfluidics and optical techniques for application in rheometry. Its major limitations are related to the capacity of the piezopumps and the pressure transducers, as well as the size of the cross-slot cell, which define the limits of the scale ranges and resolution for the imposed strain rates, inertial forces (Reynolds number) and pressure drop (Odell and Carrington 2006). We note that in the cross-slot chamber the planar extensional flow is not ideal, due to the shear component introduced by the bounding walls.

Computational rheologists have also shown interest in the cross-slot cell for assessing the performance of constitutive models, through comparison with experimental results (Rommelgas et al. 1999), or for gaining insight about purely elastic flow instabilities (Poole et al. 2007). Alves (2008) presented an integrated optimization algorithm able to find an efficient design of the shape of the flow geometry in order

Fig. 8 Illustration of the EFOR set-up. Reprinted from Odell and Carrington (2006), Copyright (2006), with permission from Elsevier Science

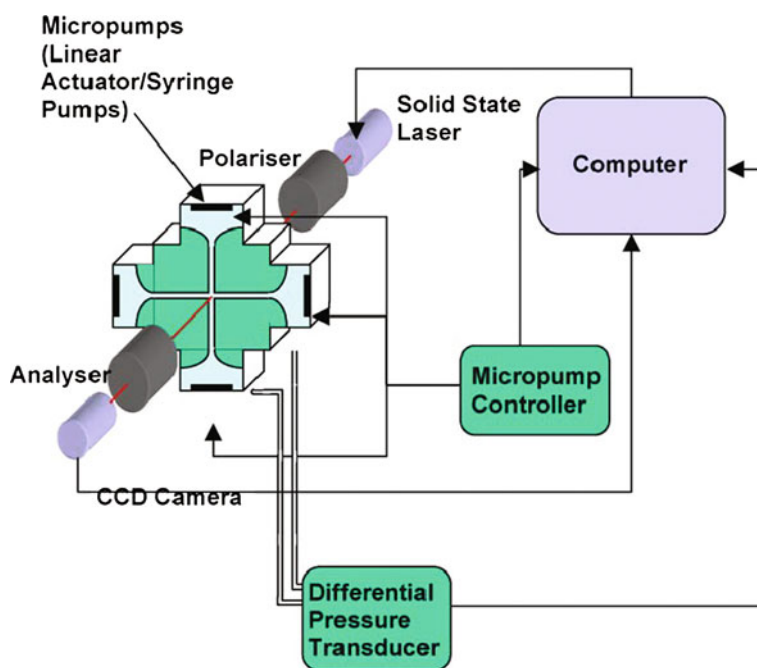
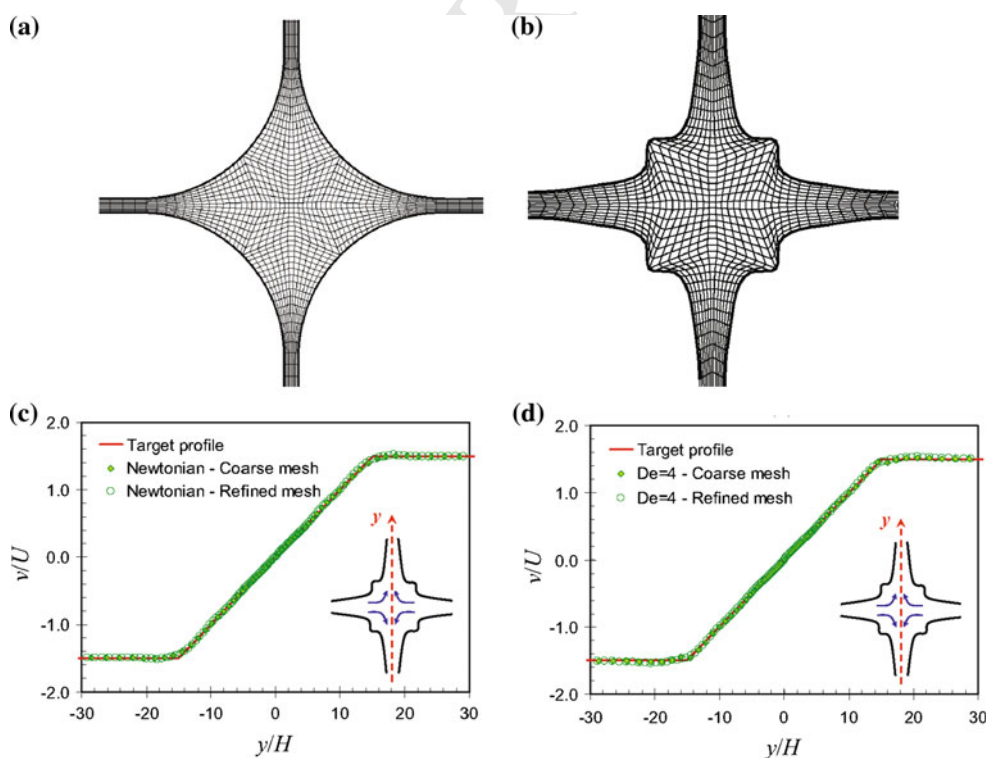


Fig. 9 Illustration of the **a** initial flow configuration, **b** the optimized flow geometry obtained using an optimal shape design technique and **c, d** the numerically predicted velocity profiles along the vertical centerline for Newtonian and viscoelastic fluids. Reprinted with permission from Alves, (2008), Copyright (2008), American Institute of Physics



496 to achieve optimal performance. The standard two-dimensional
 497 cross-slot with rounded corners was used by Alves
 498 (2008) as initial guess and the optimal shape of the chamber
 499 was determined in order to obtain an ideal planar extensional
 500 flow along the flow centerlines (see Fig. 9). Recently, the
 501 optimized microfluidic device was shown to achieve a quasi-
 502 homogeneous elongational flow, a crucial requirement to

produce meaningful rheological measurements (Haward 503
 et al. 2012b). 504

2.1.3 T-shaped microchannels 505

T-shaped microchannels have been used for multiple pur- 506
 poses, including the generation of micro-droplets in 507

Fig. 10 Comparison of experimental pathlines and numerical simulations (blue solid lines) using the simplified Phan-Thien-Tanner (sPTT) for the microchannels **a** with and **b** without cavity under the same flow conditions. Reprinted from Soulages et al. (2009b), Copyright (2009), with permission from Elsevier Science (color figure online)

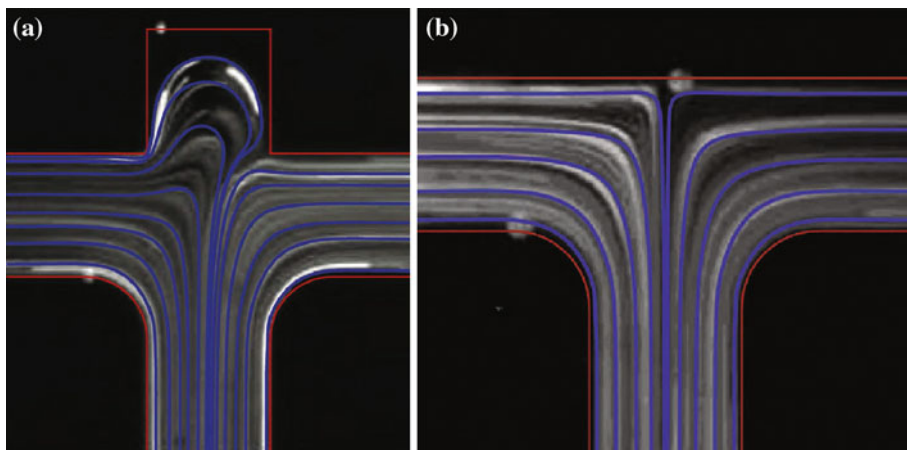
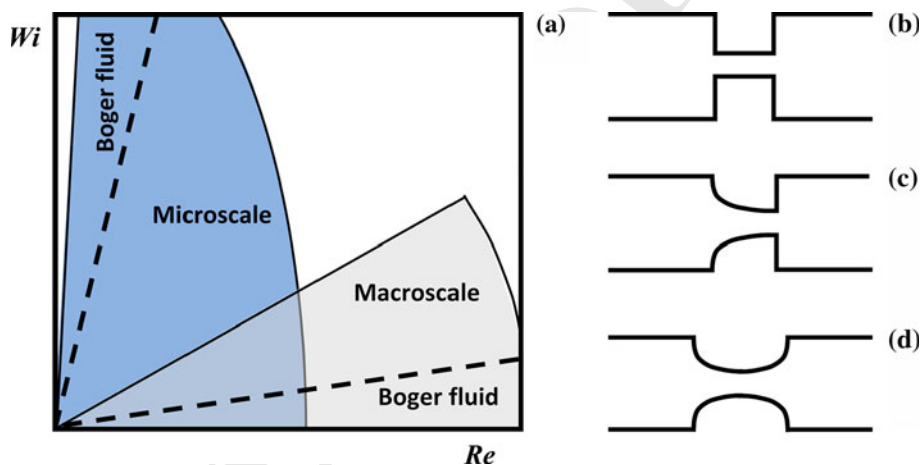


Fig. 11 a Operational regions in the $Wi-Re$ parameter space and **b-d** sketch of several canonical contraction-expansion arrangements investigated at the microscale using complex fluids Adapted from Oliveira et al. (2012)



508 microfluidic devices (Husny and Cooper-White 2006), the
 509 study of elastic driven instabilities (Soulages et al. 2009b),
 510 and for use as passive micro-mixers (Hsieh and Huang 2008).
 511 Soulages et al. (2009b) used two distinct T-shaped micro-
 512 channels (with and without a small cavity), as illustrated in
 513 Fig. 10, to investigate the onset of elastically driven flow
 514 asymmetries in steady strong extensional flows. Numerical
 515 computations and experiments using streak-imaging and
 516 micro-particle image velocimetry (μ PIV) with the T-shaped
 517 microchannels showed good agreement and allowed to gain
 518 insights about the influence of kinematics near the stagnation
 519 point in the resulting polymeric stress fields, and control the
 520 critical conditions and spatio-temporal dynamics of the
 521 resulting viscoelastic flow instabilities. Despite the partial
 522 success in the simulation of complex fluid flow in T-shaped
 523 microchannels, their use for the characterization of exten-
 524 sional properties of low viscosity fluids is still unexplored.

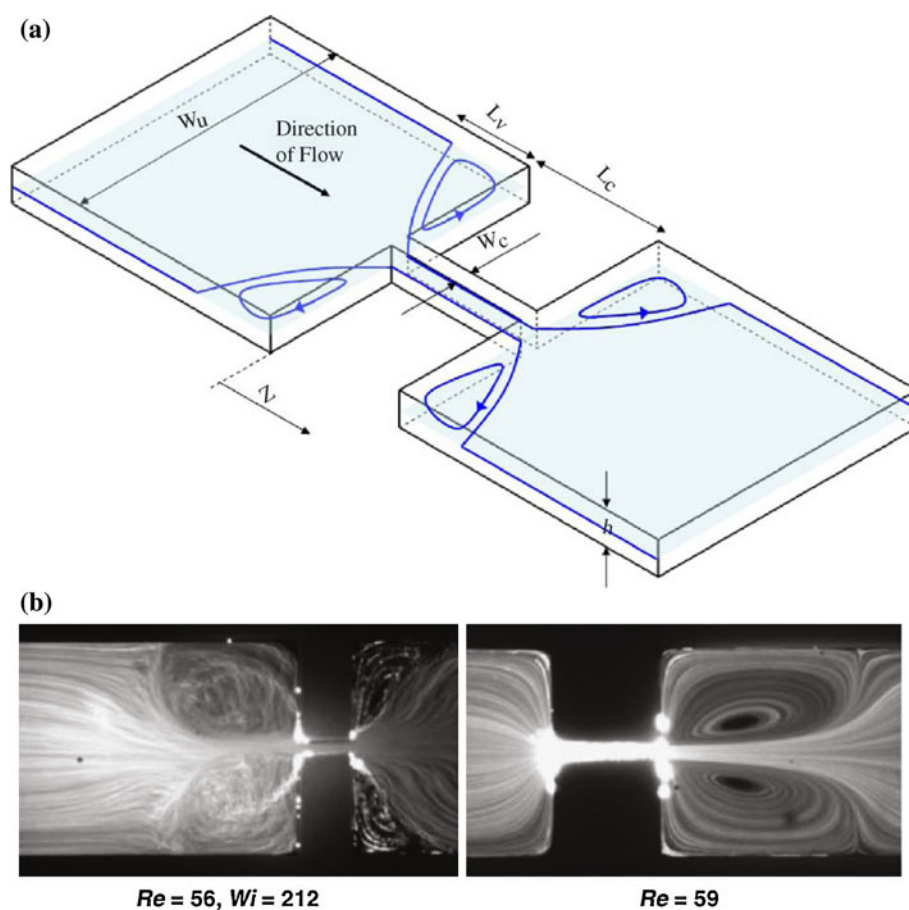
525 **2.2 Microfluidic contraction-expansion flows**

526 Even though flows of complex fluids in converging-diverg-
 527 ing microdomains may differ from their counterparts at
 528 macroscale there is a common feature: it is a complex flow

529 containing shear-dominated regions near the walls and non-
 530 homogeneous extension along the centerline, with a positive
 531 strain rate upstream of the contraction plane and a negative
 532 strain rate downstream of the expansion (Rothstein and
 533 McKinley 1999, 2001). In the pursuit of developing an
 534 efficient microfluidic rheometer-on-a-chip, capable of
 535 achieving high strain rates in such a way that it can be used
 536 to measure the extensional properties of low viscosity complex
 537 fluids, the use of a microfabricated geometry containing a
 538 contraction-expansion section is becoming a classical
 539 approach after the pioneering works of Rodd et al. (2005a,
 540 2007). At the microscale the small characteristic length-
 541 scales enhance the elasticity of the flow ($El = Wi/Re = \frac{\lambda\eta}{\rho L^2}$)
 542 and allow to reach unexplored regions in the Weissenberg
 543 number – Reynolds number ($Wi - Re$) parameter space, as
 544 shown in Fig. 11a (Rodd et al. 2007; Oliveira et al. 2012). In
 545 this section, we review the microfluidic contraction-expan-
 546 sion microgeometries frequently used in the characterization
 547 of extensional properties of low viscosity fluids, which are
 548 illustrated in Fig. 11b-d.

549 Abrupt contraction-expansion geometries have been
 550 used extensively to investigate non-linear flow phenomena
 551 associated with fluid elasticity in converging flows at the

Fig. 12 **a** Schematic diagram of the planar microfluidic contraction–expansion. **b** Comparison between Newtonian (*right*) and viscoelastic (*left*) planar entry flows at similar Re in a 16:1 contraction–expansion (flow is from *left to right*). Reprinted from Rodd et al. (2005a), Copyright (2005), with permission from Elsevier Science



552 macroscale. However, as previously mentioned, at macro-
 553 lengthscales it is not possible to characterize the exten-
 554 sional properties of low viscosity dilute polymer solutions
 555 with relaxation times of the order of milliseconds due to the
 556 small relative importance of elastic stresses compared to
 557 inertial stresses, leading to low values of the elasticity
 558 number. However, at the microscale, the elasticity number
 559 for the same fluid is much larger and it is possible to
 560 observe elastic effects in the flow patterns imaged using
 561 streak photography (Rodd et al. 2005a). Figure 12 illus-
 562 trates the formation of vortices upstream of a microfluidic
 563 planar contraction, a well-known feature of viscoelastic
 564 fluid flows (Bird et al. 1987). Furthermore, elasticity dims
 565 the formation of inertia-driven downstream vortices
 566 (Oliveira et al. 2007b; Sousa et al. 2011). Moreover, from
 567 a rheometric point of view, this geometry allows for the
 568 control of the strain rate by changing the flow rate (Oliveira
 569 et al. 2008b).

570 The ability to determine the excess pressure drop across
 571 the contraction–expansion suggests that these devices can
 572 be used to develop microfluidic extensional rheometers
 573 (Rodd et al. 2005a). However, the flow disturbance
 574 induced by the presence of the pressure taps introduced at
 575 the channel walls can lead to important errors in the

576 pressure drop measurements, an effect that is known as the
 577 pressure-hole error (Tanner 1988). To overcome this
 578 problem, pressure sensors embedded in the surface of the
 579 channels could be used as in the Rheosense VROC™ (Pipe
 580 et al. 2008). Another drawback of using the abrupt con-
 581 traction–expansion geometry as a microfluidic extensional
 582 rheometer is that the strain rate along the centerline is not
 583 constant. In order to minimize this limitation, a more
 584 interesting configuration would be a contraction–expansion
 585 with a hyperbolic shape, as shown in Fig. 13. The use of
 586 hyperbolic contractions results in a quasi-homogeneous
 587 extensional flow within the central part of the contraction
 588 geometry, and the total Hencky strain experienced by a
 589 fluid element is given by $\epsilon_H = \ln(D_1/D_2)$, where D_1 and
 590 D_2 are the widths of the large and narrow sections of the
 591 hyperbolic contraction, respectively. Higher Hencky strains
 592 lead to wider regions of *constant* strain rate in the center
 593 of the contraction, although entrance and wall effects are not
 594 totally avoided (Oliveira et al. 2007a).

595 Recently, Campo-Deaño et al. (2011) assessed the
 596 capabilities of using an hyperbolic contraction-abrupt
 597 expansion geometry as an extensional microrheometer. The
 598 relaxation times of low viscosity Boger fluids were esti-
 599 mated by means of the critical Deborah number for the

Fig. 13 Flow patterns for a 50 ppm polyacrylamide aqueous solution with 1 % NaCl at different flow rates. The flow direction is from *left to right* at the Reynolds and Deborah numbers indicated. Reprinted from Campo-Deaño et al. (2011), Copyright (2011), with permission from Elsevier Science

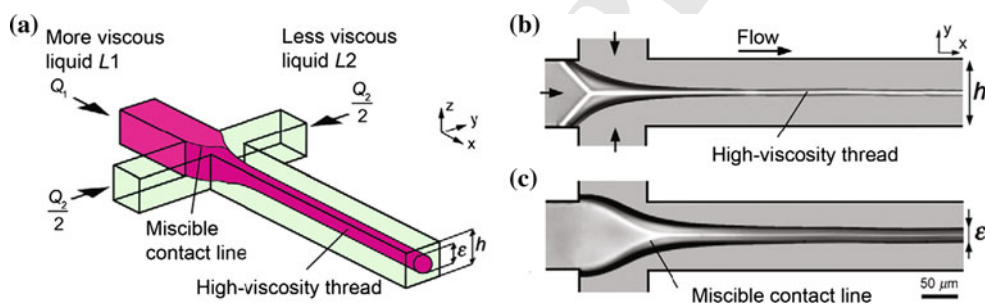
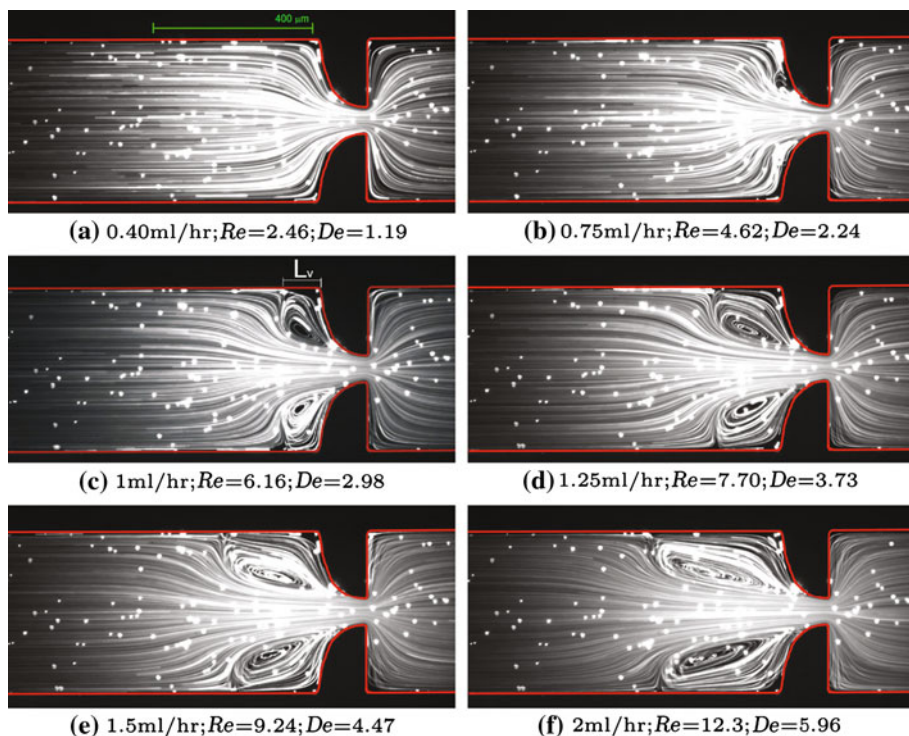


Fig. 14 Formation of threads of a core fluid lubricated with a miscible fluid. **a** Schematic three-dimensional view, **b**, **c** experimental micrographs of miscible contact lines for different flow rate ratios

($\phi = Q_1/Q_2$): **b** $\phi = 0.01$, **c** $\phi = 0.20$. Reprinted from Cubaud and Mason (2009). Copyright (2009), with permission from IOP Publishing Ltd

600 onset of secondary flow upstream of the contraction plane,
 601 which is assumed to be only weakly dependent on the
 602 polymer concentration, at least when inertial effects are
 603 negligible (see Fig. 13). One important limitation is that
 604 this microgeometry is only suitable for Boger-like fluids,
 605 since the presence of shear thinning behavior would make
 606 the analysis more complex and eventually trigger the onset
 607 of secondary flow downstream of the expansion plane.

608 2.3 Microfluidic flow focusing devices

609 In microfluidic flow focusing devices the shear effects
 610 occurring at the walls can be minimized by introducing a
 611 lubricating sheath fluid allowing to obtain a shear-free
 612 elongational flow on the core fluid, as illustrated in Fig. 14.
 613 In this section, we review different geometrical

614 configurations used in flow focusing devices with appli-
 615 cation in extensional rheometry, highlighting two key
 616 aspects for the success in the development of an exten-
 617 sional microrheometer: the miscibility between the fluids
 618 and the geometrical shape of the microfluidic device.

619 The miscibility between the core and the lubricating
 620 fluids is a crucial parameter to take into account when the
 621 working fluids are different. When the fluids are miscible,
 622 the lubricating fluid encapsulates the core fluid producing a
 623 thread, as shown in Fig. 14a. From the perspective of
 624 developing an extensional microrheometer using a flow
 625 focusing device, this is very interesting, since the lubricant
 626 fluid wraps around the core fluid and forms a thread that
 627 fully detaches from the bounding walls, generating a truly
 628 shear-free uniaxial extension, neglecting the shear in the
 629 interface between both fluids, which is a reasonable

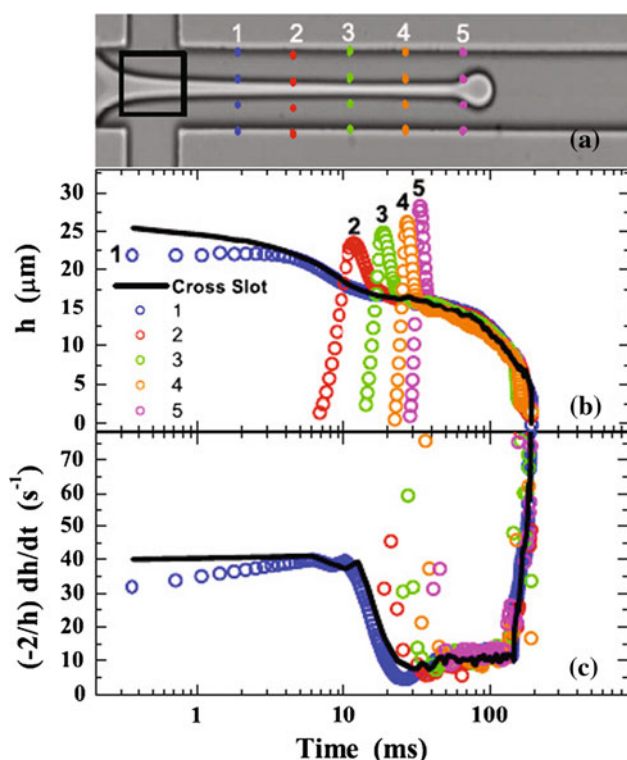


Fig. 15 **a** Filament thickness of a polyacrylamide solution, $h(t)$, measured at different locations in the cross-slot microchannel. A mineral oil is used as lubricating fluid. Measurements are performed in the central region (square) and at (dashed) lines 1–5. **b** Filament thickness of the polymeric solution at a constant flow rate measured at different locations. Data color is shown in **a**. **c** Computed extensional strain rate, $\dot{\epsilon}$, for the cases illustrated in **b**. The data show that the measurements of $h(t)$ are nearly independent of axial position, after an initial transient period. Reprinted with permission from Arratia et al. (2008). Copyright by the American Physical Society (color figure online)

630 approximation for low viscosity lubricating fluids. There
 631 is an optical signature of the thread encapsulation given
 632 by the presence of steady-state miscible contact lines, as
 633 shown in Fig. 14b, c. The encapsulation of the core fluid
 634 occurs for viscosity ratios above 15 (Cubaud and Mason
 635 2009), when the core fluid is more viscous. When the
 636 lubricating and core fluids are immiscible, a different type
 637 of thread is formed, and the core fluid remains attached
 638 to the top and bottom walls. In this situation, the shear
 639 effects from the lateral walls are reduced and a quasi-2D
 640 flow representative of planar extensional flow is gener-
 641 ated.

642 Arratia et al. (2008) used a standard cross-slot geometry
 643 to induce the stretch of viscoelastic fluids using an
 644 immiscible sheath fluid. By means of controlling the ratio
 645 between the flow rate of the core and the lubricating fluids
 646 ($q = Q_{lub}/Q_{core}$) they were able to generate filaments of the
 647 core fluid and analyzed the influence of viscoelasticity on
 648 filament thinning and breakup, as shown in Fig. 15. The

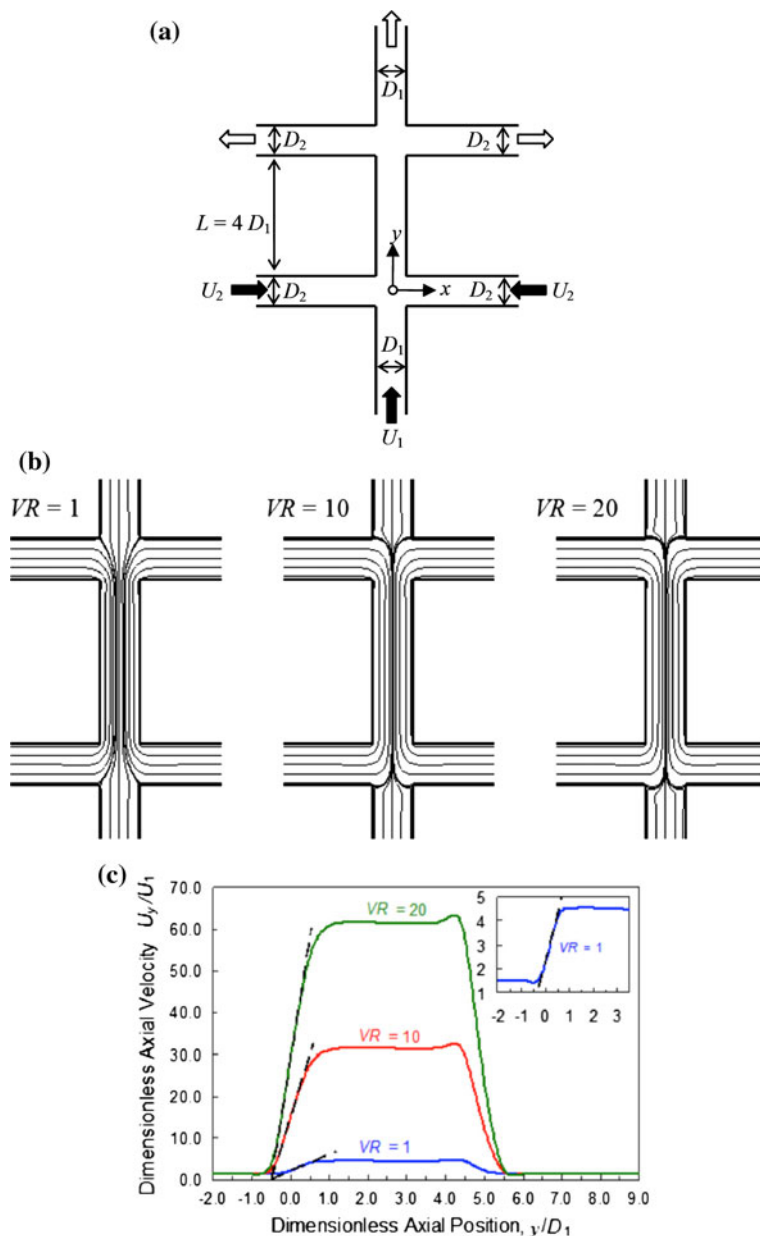
time evolution of the thickness of the filament, $h(t)$, at the
 649 mid-plane of the microchannel ($z = H/2$) was recorded and
 650 the extensional strain rate was calculated as $\dot{\epsilon} = -(2/h) \frac{dh}{dt}$.
 651 Their results suggest that the steady-state extensional vis-
 652 cosity can be estimated from the exponential rate of thin-
 653 ning. In spite of this breakthrough, one must take into
 654 account two key features for having success in the mea-
 655 surement of the steady-state extensional viscosity of the
 656 core fluid using this technique:
 657

- The generated filament of the core fluid is not a thread,
 658 as occurs in the CaBER but rather a sheet (Cubaud and
 659 Mason 2009) having the height of the channel and a
 660 thickness that varies ideally only with time. However,
 661 depending on the interfacial tension between the core
 662 and the lubricating fluids, the thickness can also vary
 663 throughout the depth of the channel.
 664
- The depth of the microchannel is also an important
 665 parameter, since the top and bottom walls of the
 666 microchannels influence the kinematics of the flow at
 667 the mid-plane. If the aspect ratio of the channel (depth/
 668 width) is not sufficiently large, it is not possible to
 669 achieve a shear-free flow at the mid-plane.
 670

671
 672 In pursuing the understanding of the interplay between
 673 viscoelasticity and surfactant dynamics in thread formation
 674 and stretching processes in a flow focusing microdevice,
 675 Lee et al. (2011) analyzed the ability of viscoelasticity to
 676 enhance the formation of jets and long threads. Their
 677 analysis focused on the control of droplet formation in flow
 678 focusing microdevices, but also showed up to what extent
 679 relaxation times extracted from thread formation depend on
 680 interfacial properties between the two fluids, which influ-
 681 ence the thread formation and breakup mechanisms and
 682 may lead to mismatching results.

683 The double-cross-slot, used by Oliveira et al. (2008a), is
 684 another promising approach to generate a shear-free exten-
 685 sional flow with nearly constant strain rate. This device
 686 consists of three entrances and three exits disposed in a
 687 symmetric configuration, as illustrated in Fig. 16a. By
 688 means of numerical calculations, Oliveira et al. (2008a)
 689 analyzed the effect of velocity ratio ($VR = U_2/U_1$, where U_1
 690 and U_2 are the inlet average velocities of the core and
 691 lubricating fluids, respectively), geometric parameter
 692 ($WR = D_2/D_1$) and Deborah number ($De = \lambda U_1/D_1$) on the
 693 flow patterns and velocity field for creeping flow conditions
 694 in two-dimensional geometries. In Oliveira et al. (2009), a
 695 similar flow focusing device with three entrances and a
 696 single exit is also analyzed numerically. One advantage of
 697 the double cross-slot is that the Hencky strain can be adjusted
 698 by varying either VR or WR, since $\epsilon_H = \ln[3(1 + 2VR \times$
 699 $WR)/2]$, and varying VR is straightforward and does not
 700 require any change to the microchannel. In this way, using

Fig. 16 **a** Sketch of the double cross-slot geometry. **b** Influence of velocity ratio (VR) on the flow patterns and **c** the axial velocity profiles along the centerline for $D_1 = D_2$ and $De = 0.2$. Reprinted with permission from Oliveira et al. (2008a), Copyright (2008), American Institute of Physics

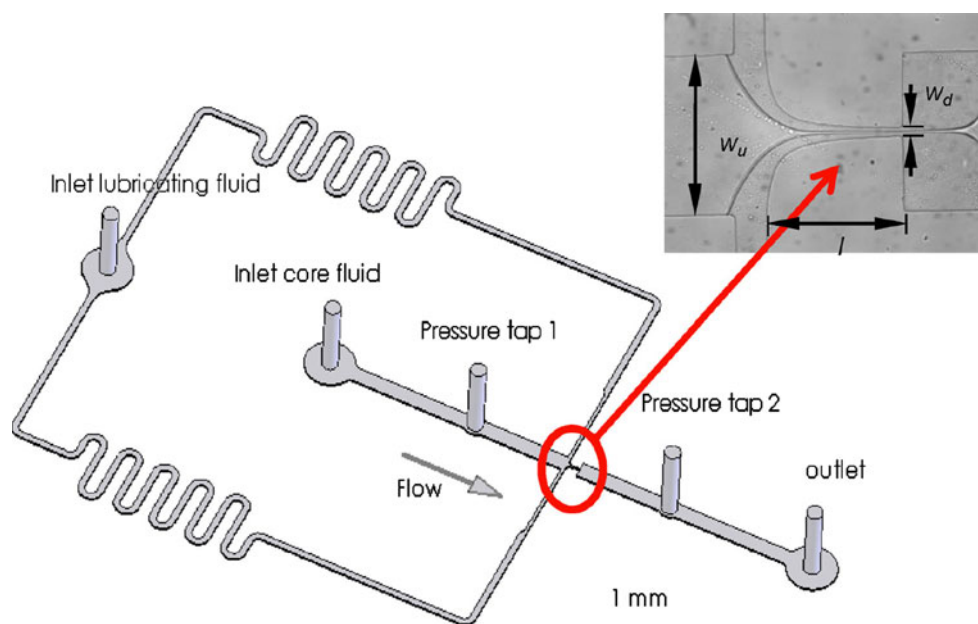


701 only one general device the user can analyze the extensional
 702 flow for a range of ϵ_H . Obviously, things are more complex in
 703 practice, since the effect of the top and bottom walls has to be
 704 taken into consideration, and that inertia might not be neg-
 705 ligible for large flow rates. However, this technique for
 706 generating extensional flows in microchannels has a great
 707 potential despite the lack of published experimental works
 708 up to date. This is, undoubtedly, an interesting and relevant
 709 area for future research.

710 Recently, Wang and James (2011) proposed an experi-
 711 mental technique to estimate the extensional viscosity of
 712 dilute polymer solutions as a function of the strain rate
 713 using flow in a lubricated, converging microchannel. This
 714 apparent extensional viscosity is calculated from the

715 difference between the measured pressure drop and the
 716 calculated pressure drop that would occur only due to shear
 717 effects in the core flow. The microdevice used consists of a
 718 central channel conducting the core fluid, which is con-
 719 nected with two side streams containing the lubricating
 720 fluid. The fluids then flow through a hyperbolic contraction
 721 and an abrupt expansion, as shown in Fig. 17. The authors
 722 analyzed the effect of miscibility of the lubricating fluid,
 723 and they concluded that flow stability relies on using an
 724 immiscible lubricant, which is crucial for assessing fluid
 725 resistance to extensional deformation. This technique is
 726 also promising as a microfluidic extensional rheometer
 727 suitable for characterizing a wide range of weakly elastic
 728 fluids.

Fig. 17 Schematic of the lubricated hyperbolic microchannel. The *inset* picture shows a viscous Newtonian fluid lubricated by water introduced through the lateral inlets. Reprinted with permission from Wang and James (2011), Copyright (2011), American Institute of Physics for the Society of Rheology



729 2.4 Electrowetting-on-dielectric microfluidic actuators

730 More than one century after the groundbreaking work in
 731 electrocapillarity by Lippmann (1875), who discovered that
 732 the capillary depression of mercury in contact with elec-
 733 trolyte solutions could be varied by changing the applied
 734 voltage between the mercury and the electrolyte (Mugele
 735 and Baret 2005), the “Electrowetting” effect was described
 736 by Beni and Hackwood (1981) with a practical application
 737 in the development of passive displays. In order to over-
 738 come the problem of electrolysis upon applying voltages
 739 beyond a few millivolts, Berge (1993) proposed to cover
 740 the metallic electrode with a thin insulate layer, which gave
 741 place to the concept of Electrowetting-on-dielectric
 742 (EWOD). Its application to microfluidics is based on the
 743 actuation of tiny amounts of liquids using the principle of
 744 modulating the interfacial tension between a liquid and an
 745 electrode coated with a dielectric layer. When the electric
 746 field is applied only to a portion of the droplet, an imbal-
 747 ance of interfacial tension is created, which forces the
 748 droplet to move (Pollack et al. 2010). Droplets are usually
 749 sandwiched between two parallel plates: the electrode array
 750 is located at the bottom plate, while the top surface is either
 751 a continuous ground plate or a passive top plate (Song
 752 et al. 2009). EWOD has become a widely used concept in
 753 various microfluidic operations including the actuation,
 754 formation, splitting, and mixing of droplets on smooth
 755 surfaces (Kumari and Garimella 2011).

756 The potential of using EWOD actuation in rheometry was
 757 demonstrated by Lin et al. (2007), who proposed a micro-
 758 viscometer based on electrowetting-on-dielectric, and Ban-
 759 purkar et al. (2009), who used EWOD to determine the
 760 elastic moduli of gelled aqueous droplets by using a sessile

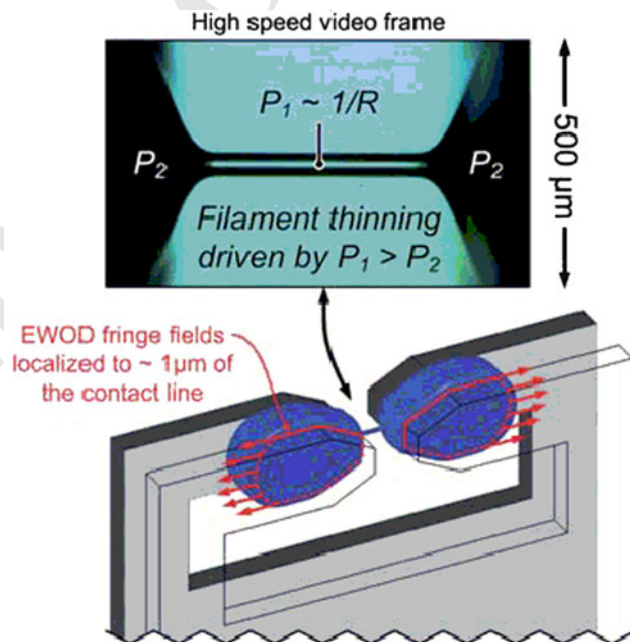


Fig. 18 Three-dimensional sketch of a loaded chip and close-up of the liquid bridge formed using EWOD activation. Reprinted with permission from Nelson et al. (2011), Copyright (2011), The Royal Society of Chemistry

761 droplet and relating liquid properties (e.g. elastic modulus) to
 762 the voltage-dependent measured contact angle. More
 763 recently, Nelson et al. (2010, 2011) went a step forward and
 764 proposed the equivalent of a miniaturized CaBER™ based
 765 on EWOD. Instead of miniaturizing the existing actuators,
 766 they took advantage of the favorable scaling of surface forces
 767 at the microscale and EWOD actuation to avoid using
 768 moving parts. Thus, depending on their electrical properties,
 769 the test samples are pulled by EWOD effects which stretch

770 the droplet as shown in Fig. 18, similar to the way in which
 771 the CaBER™ uses linear actuators to impose a step strain
 772 extending the liquid bridge.

773 This EWOD extensional rheometer exhibits the fol-
 774 lowing advantages:

- 775 • the undesired oscillations of the suspended fluid
 776 induced by inertia are minimized, as the test platform
 777 handles tiny sample volumes (Kojic et al. 2006),
- 778 • the apparatus is able to easily generate shear-free fluid
 779 filaments by either spontaneous capillary wetting or
 780 using EWOD actuation. In this scheme, the capillary
 781 breakup of a viscoelastic filament is driven by Laplace
 782 pressure, and opposed by internal shear and elasticity,
 783 without the influence of gravity or inertial-driven
 784 oscillations. Therefore, it is possible to measure com-
 785 plex fluids' properties using the known models result-
 786 ing from a balance of these dominant forces (Nelson
 787 et al. 2010),
- 788 • the shape of the sample holding platform can be designed
 789 in order to facilitate the necking process and to ensure

790 that the measurement point (i.e., the location of the
 791 minimum radius of the filament) remains fixed in space
 792 (Nelson et al. 2010), which is an advantage with regards
 793 to the design of the original CaBER™ system and

- 794 • the micro-machined chip can be easily fabricated and
 795 can be scaled down to handle sub-microliter volumes,
 796 making it especially useful for characterizing expensive
 797 materials and scarce biological fluids.

798 However, the instrument has also some limitations, such as:

- 799 • the applied voltages might influence the rheological
 800 properties of the fluid,
- 801 • the length of the initial filament is fixed for each chip,
 802 and may not be appropriate for all kinds of fluids and
- 803 • the pre-deformation history cannot be properly controlled.

2.5 Surface acoustic wave-induced fluid jetting 804

805 Tan et al. (2009) demonstrated experimentally that it is
 806 possible to generate a liquid jet ejecting up to 1–2 cm

Fig. 19 a Set-up to generate the focused SAWs whose radiation into the drop placed on the substrate focal point induces a deformation into a coherent elongated jet as shown in b–d. The water–air interface reflects the acoustic radiation throughout the vertical fluid column as illustrated in d. Reprinted with permission from Tan et al. (2009). Copyright (2009) by the American Physical Society

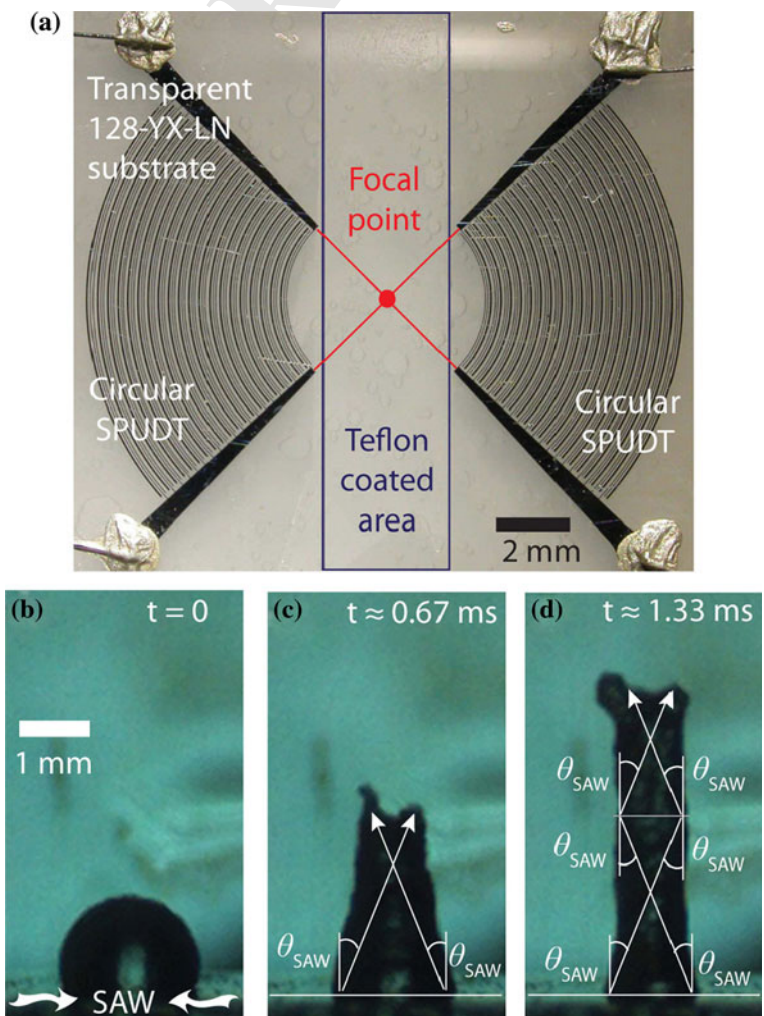
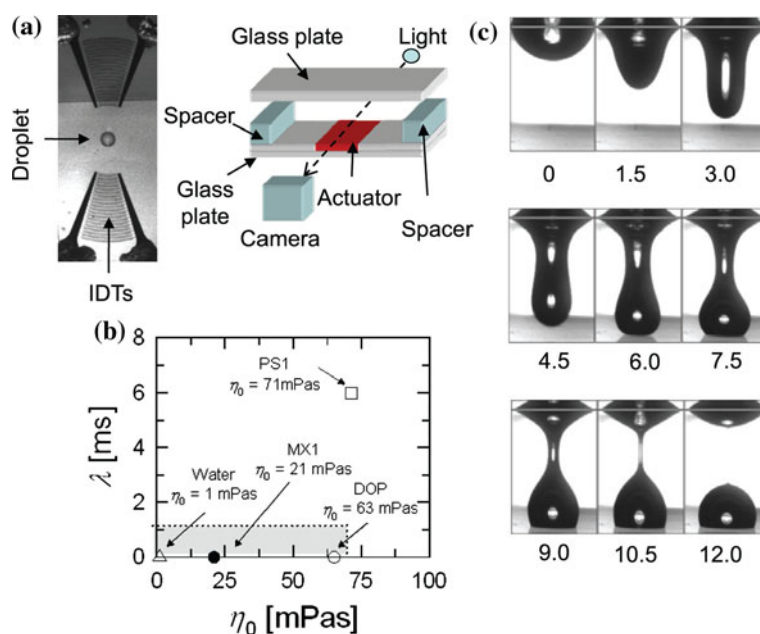


Fig. 20 **a** Set-up for SAW jetting. **b** The solutions used by Bhattacharjee et al. (2011) are shown as symbols. The shaded region in the λ - η_0 parameter space is difficult to access in conventional CaBERTM experiments. **c** Jet formation from the droplet and bridge necking down under the influence of capillary forces acting at the interface. The numbers correspond to the elapsed time in milliseconds. Reprinted from Bhattacharjee et al. (2011), Copyright (2011), with permission from IOP Publishing Ltd



807 from the free surface of a sessile drop by concentrating
 808 the energy of surface acoustic waves (SAW) into the
 809 mentioned drop (cf. Fig. 19). Based on this phenomenon,
 810 Bhattacharjee et al. (2011) were able to investigate the
 811 extensional flow of low-viscosity fluids in capillary
 812 bridges formed by pulsed surface acoustic wave jetting.
 813 Focusing electrodes at the ends of a lithium niobate piezo-
 814 electric crystal provided a focused SAW into the drop
 815 placed on the substrate at the focal point, generating a
 816 deformation in the form of a coherent elongated jet (left
 817 panel of Fig. 20). Using this principle, a liquid bridge can
 818 be created when the resulting jet touches and attaches to
 819 the top end-plate. In the experiments of Bhattacharjee
 820 et al. (2011), the setup was inverted and the droplet
 821 jet moved downwards along the direction of gravity.
 822 Figure 20c shows the time evolution of the coherent
 823 jet formed from the droplet and creation of the liquid
 824 bridge. For rheometric measurements the start time is
 825 $t_0 = 7.5$ ms, the time at which the SAW actuation ends
 826 for the experiment illustrated in Fig. 20c. Subsequently,
 827 the bridge thins under the influence of capillary forces
 828 acting at the interface. The relaxation time for different
 829 fluids are shown in Fig. 20b, illustrating that reliable
 830 measurements of Newtonian and viscoelastic fluids can be
 831 obtained in the region where the conventional CaBERTM
 832 apparatus cannot be used (grey area in Fig. 20b) due to
 833 inertia-driven oscillations, with the added advantage of
 834 using a small amount of liquid (≤ 5 μ l). However, the
 835 major drawback of this technique lies on the complex
 836 combination of operating variables (aperture of the SAW
 837 interdigital transducer, contact angle of the fluid, ampli-
 838 tude of the induced SAW and alignment of the end-plates)
 839 that must be properly controlled to significantly enhance

the reproducibility of the breakup time of liquid bridges.
 Without due care, the droplet can fail to jet and form a
 liquid bridge or even atomize.

3 Perspectives

In this review, we discuss recent advances in microfluidic
 techniques relevant for the development of an extensional
 rheometer-on-a-chip able to characterize the extensional
 properties of low viscosity elastic fluids. In recent years,
 microfluidics has evolved from being a promising platform
 for rheometry to becoming one of the most suitable
 approaches in the characterization of extensional properties
 of dilute polymer solutions at the moment. However,
 despite the great progresses, there is still much to be done
 in order to improve current techniques and, of course, there
 are also many unexplored approaches to be pursued. In
 designing and optimizing a microfluidic geometry it is
 desirable to combine experiments with numerical compu-
 tations of the corresponding flow field in order to achieve
 an ideal flow field and systematically explore the sensi-
 tivity of the kinematics to changes in the geometry and the
 flow conditions. This is arguably the best approach to
 proceed in order to succeed in the quest of designing
 efficient microfluidic extensional rheometers with optimal
 performance.

Acknowledgments The authors would like to acknowledge *Funda-
 ção para a Ciência e a Tecnologia* (FCT), COMPETE and FEDER
 for financial support through projects PTDC/EME-MFE/099109/
 2008, PTDC/EME-MFE/114322/2009, PTDC/EQU-FTT/118716/
 2010 and the scholarship SFRH/BPD/69663/2010. The authors also
 thank Dr. Rob Poole (University of Liverpool) for helpful comments.

- 871 Alves MA (2008) Design a cross-slot flow channel for extensional
872 viscosity measurements. AIP Conf Proc 1027:240–242
- 873 Anna SL, McKinley GH (2008) Effect of a controlled pre-deformation
874 history on extensional viscosity of dilute polymer solutions.
875 Rheol Acta 47:841–859
- 876 Anna SL, Rogers C, McKinley GH (1999) On controlling the
877 kinematics of a filament stretching rheometer using a real-time
878 active control mechanism. J Non Newton Fluid Mech 87:307–335
- 879 Anna SL, McKinley GH, Nguyen DA, Sridhar T, Muller S, Huang J,
880 James DF (2001) An interlaboratory comparison of measure-
881 ments from filament-stretching rheometers using common test
882 fluids. J Rheol 45(1):83–114
- 883 Ardekani AM, Sharma V, McKinley GH (2010) Dynamics of bead
884 formation, filament thinning and breakup in weakly viscoelastic
885 jets. J Fluid Mech 665:46–56
- 886 Arratia PE, Thomas CC, Diorio J, Gollub JP (2006) Elastic
887 instabilities of polymer solutions in cross-channel flow. Phys
888 Rev Lett 96:144502
- 889 Arratia PE, Gollub JP, Durian DJ (2008) Polymeric filament thinning
890 and breakup in microchannels. Phys Rev E 77:036309
- 891 Babcock HP, Teixeira RE, Hur JS, Shaqfeh ESG (2003) Visualization
892 of molecular fluctuations near the critical point of the coil-stretch
893 transition in polymer elongation. Macromolecules 36:4544–4548
- 894 Balducci AG, Tang J, Doyle PS (2008) Electrophoretic stretching of
895 dna molecules in cross-slot nanoslit channels. Macromolecules
896 41:9914–9918
- 897 Bandalusera HCH, Zimmerman WB, Rees JM (2009) Microfluidic
898 rheometry of a polymer solution by micron resolution particle
899 image velocimetry: a model validation study. Meas Sci Technol
900 20:115404
- 901 Banpurkar AG, Duits MHG, van den Ende D, Mugele F (2009)
902 Electrowetting of complex fluids: perspectives for rheometry on
903 chip. Langmuir 25:1245–1252
- 904 Bäsnsch E, Berg CP, Ohlhoff A (2004) Uniaxial extensional flows in
905 liquid bridges. J Fluid Mech 521:353–379
- 906 Barnes HA, Hutton JF, Walters K (1993) An introduction to rheology.
907 Rheology series, 3rd edn. Elsevier, The Netherlands
- 908 Bazilevsky A, Entov V, Rozhkov A (1990) Liquid filament micro-
909 rheometer and some of its applications. In: Oliver DR (ed)
910 Proceedings of the third European rheology conference. Elsevier,
911 The Netherlands, pp 41–43
- 912 Becherer P, Morozov AN, van Saarloos W (2008) Scaling of singular
913 structures in extensional flow of dilute polymer solutions. J Non
914 Newton Fluid Mech 153:183–190
- 915 Beni G, Hackwood S (1981) Electro-wetting displays. Appl Phys Lett
916 38(4):207–209
- 917 Berge B (1993) Electrocapillarité et mouillage de films isolants par
918 l'eau. Comptes rendus de l' Academie des sciences Serie 2
919 317(2):157–163
- 920 Bhattacherjee PK, McDonnell AG, Prabhakar R, Yeo LY, Friend J
921 (2011) Extensional flow of low-viscosity fluids in capillary
922 bridges formed by pulsed surface acoustic wave jetting. New J
923 Phys 13:023005
- 924 Bird RB, Armstrong RC, Hassager O (1987) Dynamics of polymer
925 liquids. Fluid mechanics, vol 1, 2nd edn. Wiley, USA
- 926 Campo-Deaño L, Clasen C (2010) The slow retraction method (SRM)
927 for the determination of ultra-short relaxation times in capillary
928 breakup extensional rheometry experiments. J Non Newton Fluid
929 Mech 165:1688–1699
- 930 Campo-Deaño L, Galindo-Rosales FJ, Pinho FT, Alves MA, Oliveira
931 MSN (2011) Flow of low viscosity boger fluids through a
932 microfluidic hyperbolic contraction. J Non Newton Fluid Mech
933 166:1286–1296
- Cubaud T, Mason TG (2009) High-viscosity fluids threads in weakly
diffusive microfluidic systems. New J Phys 11:075029
- Dontula P, Pasquali M, Scriven LE, Macosko CW (1997) Can
extensional viscosity be measured with opposed-nozzle devices.
Rheol Acta 36:429–448
- Dukhin A, Zelenev A (2010) Rheology: shear, extensional, longitu-
dinal. Sci Topics. [http://www.scitopics.com/Rheology_shear_](http://www.scitopics.com/Rheology_shear_extensional_longitudinal.html)
[extensional_longitudinal.html](http://www.scitopics.com/Rheology_shear_extensional_longitudinal.html) (accessed 20 June 2012)
- Dylla-Spears R, Townsend JE, Jen-Jacobson L, Sohn LL, Muller SJ
(2010) Single-molecule sequence detection via microfluidic planar
extensional flow at a stagnation point. Lab Chip 10:1543–1549
- Erni P, Varagnat M, Clasen C, Crest J, McKinley GH (2011)
Microrheometry of sub-nanolitre biopolymer samples: non-
newtonian flow phenomena of carnivorous plant mucilage. Soft
Matter 7:10889
- Franck A (2011) The ARES-EVF: option for measuring extensional
viscosity of polymer melts. [http://www.tainstruments.com/pdf/](http://www.tainstruments.com/pdf/literature/APN002_V2_ARES_EVF_to_measure_elongation_viscosity.pdf)
[literature/APN002_V2_ARES_EVF_to_measure_elongation_](http://www.tainstruments.com/pdf/literature/APN002_V2_ARES_EVF_to_measure_elongation_viscosity.pdf)
[viscosity.pdf](http://www.tainstruments.com/pdf/literature/APN002_V2_ARES_EVF_to_measure_elongation_viscosity.pdf) (accessed 20 June 2012)
- Fuller GG, Cathey CA, Hubbard B, Zebrowski BE (1987) Extensional
viscosity measurements for low-viscosity fluids. J Rheol
31:235–249
- Funami T (2011) Next target for food hydrocolloid studies: texture
design of foods using hydrocolloid technology. Food Hydrocol-
loids 25:1904–1914
- Gaudet S, McKinley GH (1998) Extensional deformation of non-
Newtonian liquid bridges. Comput Mech 21:461–476
- Göttfert (2011) Elongational testing—rheotens and haul-off.
[http://www.goettfert.com/images/stories/downloads/produkte/](http://www.goettfert.com/images/stories/downloads/produkte/Rheotens_71-97_en.pdf)
[Rheotens_71-97_en.pdf](http://www.goettfert.com/images/stories/downloads/produkte/Rheotens_71-97_en.pdf) (accessed 20 June 2012)
- Guillot P, Panizza P, Salmon JP, Joanicot M, Colin A (2006)
Viscosimeter on a microfluidic chip. Langmuir 22:6438–6445
- Guillot P, Moulin T, Kotitz RMG, Dodge A, Joanicot M, Colin A,
Bruneau CH, Colin T (2008) Towards a continuous microfluidic
rheometer. Microfluid Nanofluid 5:619–630
- Gupta RK, Sridhar T (1988) Rheological Measurements. In: Clegg D,
Collyer AA (eds) Elsevier, The Netherlands
- Haward SJ (2010) Buckling instabilities in dilute polymer solution
elastic strands. Rheol Acta 49:1219–1225
- Haward SJ, Odell JA, Berry M, Hall T (2011) Extensional rheology of
human saliva. Rheol Acta 50:869–879
- Haward SJ, Ober TJ, Oliveira MSN, Alves MA, McKinley GH
(2012a) Extensional rheology and elastic instabilities of a
wormlike micellar solution in a microfluidic cross-slot device.
Soft Matter 8:536–555
- Haward SJ, Oliveira MSN, Alves MA, McKinley GH (2012b)
Optimized cross-slot flow geometry for microfluidic extensional
rheometry. Phys Rev Lett (submitted)
- Hermansky CG, Boger DV (1995) Opposing-jet viscometry of fluids
with viscosity approaching that of water. J Non Newton Fluid
Mech 56:1–14
- Hsieh SS, Huang YC (2008) Passive mixing in micro-channels with
geometric variations through μ PIV and μ LIF measurements.
J Micromech Microeng 18:065017
- Hudson SD, Phelan FR, Handler MD, Cabral JT, Migler KB, Amis EJ
(2004) Microfluidic analog of the four-roll mill. Appl Phys Lett
85(2):335–337
- Husny J, Cooper-White JJ (2006) The effect of elasticity on drop
creation in T-shaped microchannels. J Non Newton Fluid Mech
137:121–136
- Kojic N, Bico J, Clasen C, McKinley GH (2006) *Ex vivo* rheology of
spider silk. J Exp Biol 209:4355–4362
- Kumari N, Garimella SV (2011) Electrowetting-induced dewetting
transitions on superhydrophobic surfaces. Langmuir 27:10342–
10346

- 999 Lagnado RR, Leal LG (1990) Visualization of three-dimensional flow
1000 in a four-roll mill. *Exp Fluids* 9:25–32
- 1001 Lee JS, Dylla-Spears R, Teclerian NP, Muller SJ (2007)
1002 Microfluidic four-roll mill for all flow types. *Appl Phys Lett*
1003 90:074103
- 1004 Lee W, Walker LM, Anna SL (2011) Competition between visco-
1005 elasticity and surfactant dynamics in flow focusing microfluidics.
1006 *Macromol Mater Eng* 296:203–213
- 1007 Lin YY, Lin CW, Yang LJ, Wang AB (2007) Micro-viscometer based
1008 on electrowetting on dielectric. *Electrochim Acta* 52:2876–2883
- 1009 Link DR, Anna SL, Weitz DA, Stone HA (2004) Geometrically
1010 mediated breakup of drops in microfluidic devices. *Phys Rev*
1011 *Lett* 92(5):054503
- 1012 Lippmann G (1875) Relations entre les phénomènes électriques et
1013 capillaires. *Ann Chim Phys* 5:494
- 1014 Macosko CW (1994) *Rheology: principles, measurements, and*
1015 *applications*. Wiley, USA
- 1016 Maia JM, Covas JA, Nóbrega JM, Dias TF, Alves FE (1999)
1017 Measuring uniaxial extensional viscosity using a modified
1018 rotational rheometer. *J Non Newton Fluid Mech* 80:183–197
- 1019 Matta JE, Tytus RP (1990) Liquid stretching using a falling cylinder.
1020 *J Non Newton Fluid Mech* 35:215–229
- 1021 McKinley GH (2005) Visco-elasto-capillary thinning and break-up of
1022 complex fluids. In: Binding DM, Walters K (eds) *Rheology*
1023 *reviews*. The British Society of Rheology
- 1024 McKinley GH, Hall NR (2011a) Shear history extensional rheology
1025 experiment II (SHERE II). [http://issresearchproject.grc.nasa.gov/](http://issresearchproject.grc.nasa.gov/MSG/SHERE_II/)
1026 [MSG/SHERE_II/](http://issresearchproject.grc.nasa.gov/MSG/SHERE_II/) (accessed 20 June 2012)
- 1027 McKinley GH, Hall NR (2011b) Shear history extensional rheology
1028 experiment (SHERE). [http://issresearchproject.grc.nasa.gov/](http://issresearchproject.grc.nasa.gov/MSG/SHERE/)
1029 [MSG/SHERE/](http://issresearchproject.grc.nasa.gov/MSG/SHERE/) (accessed 20 June 2012)
- 1030 McKinley GH, Sridhar T (2002) Filament-stretching rheometry of
1031 complex fluids. *Annu Rev Fluid Mech* 34:375–415
- 1032 McKinley GH, Tripathi A (2000) How to extract the Newtonian
1033 viscosity from capillary breakup measurements in a filament
1034 rheometer. *J Rheol* 44(3):653–671
- 1035 McKinley GH, Brauner O, Yao M (2001) Kinematics of filament
1036 stretching in dilute and concentrated polymer solutions. *Korea*
1037 *Austral J Rheol* 13(1):29–35
- 1038 Meissner J (1985a) Experimental aspects in polymer melt elonga-
1039 tional rheometry. *Chem Eng Commun* 33:159–180
- 1040 Meissner J (1985b) Rheometry of polymer melts. *Annu Rev Fluid*
1041 *Mech* 17:45–64
- 1042 Mugele F, Baret JC (2005) Electrowetting: from basics to applica-
1043 tions. *J Phys Condens Matter* 17:R705–R774
- 1044 Münsted H (1979) New universal extensional rheometer for polymer
1045 melts. Measurements on a polystyrene sample. *J Rheol*
1046 23(4):421–436
- 1047 Nelson WC, Kavehpour HP, Kim CJ (2010) A micro extensional
1048 filament rheometer enabled by EWOD. In: *IEEE 23rd interna-*
1049 *tional conference on micro electro mechanical systems (MEMS)*,
1050 pp 75–78
- 1051 Nelson WC, Kavehpour HP, Kim CJ (2011) A miniature capillary
1052 breakup extensional rheometer by electrostatically assisted
1053 generation of liquid filaments. *Lab Chip* 11:2424–2431
- 1054 Ng SL, Mun RP, Boger DV, James DF (1996) Extensional viscosity
1055 measurements of dilute polymer solutions of various polymers.
1056 *J Non Newton Fluid Mech* 65:291–298
- 1057 Niedzwiedz K, Arnolds O, Willenbacher N, Brummer R (2009) How
1058 to characterize yield stress fluids with capillary breakup exten-
1059 sional rheometry (CaBER). *Appl Rheol* 19(4):41969
- 1060 Niedzwiedz K, Buggisch H, Willenbacher N (2010) Extensional
1061 rheology of concentrated emulsions as probed by capillary
1062 breakup elongational rheometry (CaBER). *Rheol Acta*
1063 49:1103–1116
- Nijenhuis K, McKinley GH, Spiegelberg S, Barnes HA, Aksel N, Heymann L, Odell JA (2007) *Springer handbook on experimental fluid mechanics*, Chap 9. Non-Newtonian flows. Springer, Berlin
- Odell JA, Carrington SA (2006) Extensional flow oscillatory rheometry. *J Non Newton Fluid Mech* 137:110–120
- Oliveira MSN, McKinley GH (2005) Iterated stretching and multiple beads-on-a-string phenomena in dilute solutions of highly extensible flexible polymers. *Phys Fluids* 17:071704
- Oliveira MSN, Yeh R, McKinley GH (2006) Iterated stretching, extensional rheology and formation of beads-on-a-string structures in polymer solutions. *J Non Newton Fluid Mech* 137:137–148
- Oliveira MSN, Alves MA, Pinho FT, McKinley GH (2007a) Viscous flow through microfabricated hyperbolic contractions. *Exp Fluids* 43:437–451
- Oliveira MSN, Oliveira PJ, Pinho FT, Alves MA (2007b) Effect of contraction ratio upon viscoelastic flow in contractions: the axisymmetric case. *J Non Newton Fluid Mech* 147:92–108
- Oliveira MSN, Alves MA, Pinho FT (2008a) Extensional effects in viscoelastic fluid flow through a micro-scale double cross-slot. *AIP Conf Proc* 1027:982–984
- Oliveira MSN, Rodd LE, McKinley GH, Alves MA (2008b) Simulations of extensional flow in microrheometric devices. *Microfluid Nanofluid* 5:809–826
- Oliveira MSN, Pinho FT, Poole RJ, Oliveira PJ, Alves MA (2009) Purely-elastic flow asymmetries in flow focusing devices. *J Non Newton Fluid Mech* 160:31–39
- Oliveira MSN, Alves MA, Pinho FT (2012) *Transport and mixing in laminar flows: from microfluidics to oceanic currents*, Chap 6. *Microfluidic flows of viscoelastic fluids*. Wiley, New York
- Padmanabhan M (1995) Measurement of extensional viscosity of viscoelastic liquid foods. *J Food Eng* 25:311–327
- Padmanabhan M, Bhattacharya M (1993) Planar extensional viscosity of corn meal dough. *J Food Eng* 18:389–411
- Pathak JA, Hudson SD (2006) Rheo-optics of equilibrium polymer solutions: wormlike micelles in elongational flow in a microfluidic cross-slot. *Macromolecules* 39:8782–8792
- Perkins TT, Smith DE, Chu S (1997) Single polymer dynamics in an elongation flow. *Science* 314:216–221
- Petrie CJS (1997) Three-dimensional presentation of extensional flow data. *J Non Newton Fluid Mech* 70:205–218
- Petrie CJS (2006) Extensional viscosity: a critical discussion. *J Non Newton Fluid Mech* 137:15–23
- Phelan FR Jr, Hudson SD, Handler MD (2005) Fluid dynamics analysis of channel flow geometries for materials characterization in microfluidic devices. *Rheol Acta* 45:59–71
- Pipe C, McKinley GH (2009) Microfluidic rheometry. *Mech Res Commun* 36:110–120
- Pipe C, Majmudar TS, McKinley GH (2008) High shear rate viscometry. *Rheol Acta* 47:621–642
- Pollack MG, Fair RB, Shenderov AD (2010) Electrowetting-based actuation of liquid droplets for microfluidic applications. *Appl Phys Lett* 96:1725–1727
- Poole RJ, Alves MA, Oliveira PJ (2007) Purely elastic flow asymmetries. *Phys Rev Lett* 99:164503
- Rommelgas J, Singh P, Leal LG (1999) Computational studies of nonlinear elastic dumbbell models of booger fluids in a cross-slot flow. *J Non Newton Fluid Mech* 88:31–61
- Ríos S, Díaz J, Galindo A, Soto E, Calderas F, Mena B (2002) Instrumentation and start up of a new elongational rheometer with preshearing history. *Rev Sci Instrum* 73:3007–3011
- Roche M, Kellay H, Stone HA (2011) Heterogeneity and the role of normal stresses during the extensional thinning of non-Brownian shear-thickening fluids. *Phys Rev Lett* 107:34503

- 1129 Rodd LE, Scott TP, Boger DV, Cooper-White JJ, McKinley GH
 1130 (2005a) The inertio-elastic planar entry flow of low-viscosity
 1131 elastic fluids in micro-fabricated geometries. *J Non Newtonian*
 1132 *Fluid Mech* 129:1–22
- 1133 Rodd LE, Scott TP, Cooper-White JJ, McKinley GH (2005b)
 1134 Capillary break-up rheometry of low-viscosity elastic fluids.
 1135 *Appl Rheol* 15:12–27
- 1136 Rodd LE, Cooper-White JJ, Boger DV, McKinley GH (2007) The
 1137 role of elasticity number in the entry flow of dilute polymer
 1138 solutions in micro-fabricated contraction geometries. *J Non*
 1139 *Newtonian Fluid Mech* 143:170–191
- 1140 Rothstein JP (2008) Strong flows of viscoelastic wormlike micelle
 1141 solutions. In: Binding DM, Walters K (eds) *Rheology reviews.*
 1142 *The British Society of Rheology*
- 1143 Rothstein JP, McKinley GH (1999) Extensional flow of a polystyrene
 1144 boger fluid through a 4:1:4 axisymmetric contraction/expansion.
 1145 *J Non Newton Fluid Mech* 86:61–88
- 1146 Rothstein JP, McKinley GH (2001) The axisymmetric contraction–
 1147 expansion: the role of extensional rheology on vortex growth
 1148 dynamics and the enhanced pressure drop. *J Non Newton Fluid*
 1149 *Mech* 98:33–63
- 1150 Sattler R, Wagner C, Eggers J (2008) Blistering pattern and formation
 1151 of nanofibers in capillary thinning of polymer solutions. *Phys*
 1152 *Rev Lett* 100:164502
- 1153 Schultz WW, Davis SH (1982) One-dimensional liquid fibers. *J Rheol*
 1154 26(4):331–345
- 1155 Schweizer T (2000) The uniaxial elongational rheometer rme—six
 1156 years of experience. *Rheol Acta* 39:428–443
- 1157 Sentmanat M, Wang BN, McKinley GH (2005) Measuring the
 1158 transient extensional rheology of polyethylene melts using the
 1159 ser universal testing platform. *J Rheol* 49(3):585–606
- 1160 Shaqfeh ESG (2005) The dynamics of single-molecule dna in flow.
 1161 *J Non Newton Fluid Mech* 130:1–28
- 1162 Song JH, Evans R, Lin YY, Hsu BN, Fair RB (2009) A scaling model
 1163 for electrowetting-on-dielectric microfluidic actuators. *Micro-*
 1164 *fluid Nanofluid* 7:75–89
- 1165 Soulages J, Le Goupil F, Hostettler J, McKinley GH (2009a) An
 1166 opposed-nozzle fixture for measuring the extensional properties
 of low viscosity liquids using a conventional controlled strain
 rheometer. In: Co A (ed) *The Society of Rheology. 81st annual*
meeting program and abstracts, p 115
- Soulages J, Oliveira MSN, Sousa PC, Alves MA, McKinley GH
 (2009b) Investigating the stability of viscoelastic stagnation
 flows in t-shaped microchannels. *J Non Newton Fluid Mech*
 163:9–24
- Sousa PC, Coelho PM, Oliveira MSN, Alves MA (2011) Laminar
 flow in three-dimensional square–square expansion. *J Non*
Newton Fluid Mech 166:1033–1048
- Squires TM, Mason TG (2010) Fluid mechanics of microrheology.
Annu Rev Fluid Mech 42:413–438
- Squires TM, Quake SR (2005) Microfluidics: fluid physics at the
 nanoliter scale. *Rev Mod Phys* 77:977–1026
- Sridhar T (2000) From rheometry to rheology. *Korea Austral Rheol J*
 12(1):39–53
- Tan MK, Friend JR, Yeo LY (2009) Interfacial jetting phenomena
 induced by focusing surface vibrations. *Phys Rev Lett*
 103:024501
- Tanner RI (1988) Pressure-hole errors—an alternative approach.
J Non Newtonian Fluid Mech 28:309–318
- Tanyeri M, Johnson-Chavarria EM, Schroeder CM (2010) Hydrody-
 namic trap for single particles and cells. *Appl Phys Lett*
 96:224101
- Tanyeri M, Ranka M, Sittipolkul N, Schroeder CM (2011) A
 microfluidic-based hydrodynamic trap: design and implementa-
 tion. *Lab Chip* 11:1786–1794
- Taylor GI (1934) The formation of emulsions in definable fields of
 flow. *Proc Roy Soc Lond Ser A* 146:501–523
- Trouton FT (1906) On the coefficient of viscous traction and its
 relation to that of viscosity. *Proc Roy Soc Lond* 77:426–440
- Wang J, James DF (2011) Lubricated extensional flow of viscoelastic
 fluid in a convergent microchannel. *J Rheol* 55:1103–1126
- Whitesides GM (2006) The origins and future of microfluidics.
Nature 42:368–370
- Zheng R, Tanner RI, Fan XJ (2011) *Injection molding: integration of*
theory and modeling methods. Springer, Berlin